63-4-1

406 924

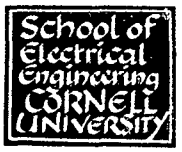

CORNELL UNIVERSITY

SCHOOL OF ELECTRICAL ENGINEERING

RESEARCH REPORT EE 547

Ballistic Analysis of Modulated Electron Beams

30 October 1962

I. Turkekul

LINEAR BEAM MICROWAVE TUBES, Technical Report No. 24 [Contract No. AF30(602)-2573]

School of Electrical Engineering
CORNELL UNIVERSITY
Ithaca, New York

RESEARCH REPORT EE 547

BALLISTIC ANALYSIS OF MODULATED ELECTRON BEAMS

I. Turkekul

LINEAR BEAM MICROWAVE TUBES

Technical Report No. 24 30 October 1962

Published under Contract No. AF30(602)-2573
Rome Air Development Center, Griffiss Air Force Base, New York

ACKNOWLEDGMENTS

The author wishes to express his gratitude to the following individuals and organizations for their assistance during the course of the investigation: to Professor G. C. Dalman, Chairman of his Special Committee, for his constant guidance and many helpful suggestions; to Professors L. F. Eastman, R. P. Agnew, and P. R. McIsaac for their advice on a course of study; to the Rome Air Development Center of the Air Research and Development Command, USAF for its support of the investigation; and to the Turkish navy for its scholarship and extended leave.

TABLE OF CONTENTS

LIST OF ILLUSTRATIONS

LIST OF SYMBOLS

d	modulating cavity gap separation
d_n	gap separation of n^{th} cavity
i	a-c current
I_o	d-c current
J_λ	intensity of X-ray radiation of wavelength λ
l_n	length of n^{th} drift space
P_k	kinetic power
t	time
v	a-c velocity
v_o	d-c velocity
V_o	d-c beam voltage
V_n	voltage across the gap of n^{th} cavity
W	normalized total kinetic energy per cycle
W_k	total kinetic energy per cycle
X	bunching parameter in the first drift space
z	axial co-ordinate

Z	normalized axial co-ordinate
α_n	depth of modulation for n^{th} cavity
β_1	phase angle of the fundamental current at plane c
β_p	ω_p/u_o
Γ_n	phase angle of the voltage across the n^{th} cavity
δ	transit angle correction factor
η	efficiency (defined as the ratio of total kinetic energy taken out of n^{th} cavity to the total kinetic energy of the electron beam at the entrance to the second gap).
θ	total transit angle of the modulating cavity
θ_{o_n}	n^{th} drift-space angle
θ_{g_n}	d-c transit angle of the n^{th} cavity
λ	wavelength of the X-ray radiation
ξ	total phase angle of the voltage across the first cavity
ϕ	total phase angle of the fundamental current at plane c
ω	frequency of input signal to modulating cavity

ABSTRACT

This report describes a ballistic analysis made of an electron beam in a two-cavity klystron, which was assumed to have infinite cross section, negligible space charge, nonrelativistic velocities, and gridded finite gaps. The operating parameters of a catcher gap for maximum efficiency and the velocity-filtering capabilities of a r-f gap interacting with a spent beam, at large signals were investigated. The term "velocity-filtering" means a reduction in the velocity of bunched electrons of a certain velocity-class. All the characteristics in this study were computed by a Burroughs Datatron 220 digital computer, when necessary.

The behavior of an electron beam in a buncher gap was investigated using a graphic analysis based on the results given by the digital computer. The velocity and current distributions emerging from this gap were formulated. The graphic results were approached by successively approximating the transit-time correction factor.

The results obtained by successive approximation were then used as initial conditions in analyzing the behavior of the electron beam in the first drift space. A Fourier series was derived which describes the various harmonics of the beam current as functions of the operating parameters of the buncher gap and the drift space, for large signals. The results are found to be in agreement with those in the literature.

The exit current and the exit velocity from the second gap were formulated as implicit functions of entrance and exit times in forms applicable to a digital computer, and the operating conditions of the second gap were taken as parameters. The computer data were sorted for both a

catcher gap and a velocity-filter gap by kinetic energy calculations. The catcher gap selected had an efficiency of 23.995 per cent.

The same procedure was applied to a second drift space and then to a third gap, so that the solutions corresponded to a combination consisting of a two-cavity klystron and a velocity-filter cavity. With the known operating parameters of the catcher gap and the velocity-filter gap, the value of the second drift angle for best filtering was determined. The velocity-filter gap selected had an efficiency of 5.368 per cent. The addition of the velocity-filter gap was shown to decrease the intensities of X-ray radiation through a given shield.

I. INTRODUCTION

The ballistic approach for analyzing an electron beam in a velocity-modulated tube was first introduced by Webster.[1] Although his theory lacks validity at or after crossover because of space-charge forces and does not apply to electron beams of finite radius because of fringing of the space-charge fields, it has two advantages: (1) It is simple and provides an insight into the physical phenomena and thus serves as a guide for more complicated theories, and (2) it is fairly accurate at large-signal levels for low-perveance beams.

The current tendency to demand higher power levels from klystrons increases the importance of ballistic theory. In an experiment, Mihran[2] showed that for large signals, the electron beam showed ballistic behavior; i.e., the debunching effect of the space-charge forces became less important. At the same time, in finite beams, the space-charge forces acted to enhance bunching at large signals by debunching inner and outer electrons differently.

In a high-power klystron, the velocity spread of the electrons in the beam increases considerably at large signals. Hard X-rays emanate from the collector of such a tube since the fast electrons reach velocities that are capable of producing these X-rays. This is a serious disadvantage of high-power klystrons, but it can, however, be overcome by devising some means of obtaining electronic interaction with the spent beam, the beam after the catcher gap. The well-known method of the d-c retarding field alone, i.e., application of a negative voltage to the collector, would not suffice, since the d-c retarding field may turn back some of the

slow electrons while decelerating the fast electrons. A r-f circuit, such as a r-f gap or a helix, on the other hand, can be designed to interact with the beam in such a way that only the fast electrons are decelerated. Such a r-f gap is analyzed in this study, and it is called the velocity-filter gap. A proper combination of the d-c and the r-f methods, then, may prevent radiation of X-rays.

The purpose of this study is to analyze the electron beam in a two-cavity klystron, using a ballistic approach, to determine the characteristics of the spent beam and to investigate the velocity-filtering capabilities of a r-f gap. To simplify this analysis a model is chosen with the following assumptions: (1) beam of infinite cross section, (2) negligible space charge, (3) gridded finite gaps, and (4) nonrelativistic velocities. All the characteristics in this study are computed by a Burroughs Datatron 220 digital computer when necessary.

The analysis of the first gap is given in Chapter II. First a graphic analysis is made by setting up exact equations for the gap and solving them with the computer; then analytical formulas are derived for the exit velocity and the exit current. These derivations are based on successive approximations to the transit time and are compared with the graphic analysis to determine the range of validity.

The results of Chapter II are used as initial conditions in Chapter III for the analysis of the drift space. Fourier analysis of the current at the end of the drift space results in a series which describes the various harmonics of the current as functions of the operating parameters of the first gap and the drift space for large signals. At this point, however, multivalued functions resulting from the occurrence of overtaking come into play, and explicit

analytical formulas no longer approximate exact formulas. In the rest of the analysis, therefore, one is restricted to dealing with exact implicit formulas.

In Chapter IV, the second gap is treated in the same way as the first gap. A r-f voltage is assumed across the second gap with variable amplitude and phase. The characteristics of the spent beam are determined by the computer and the results are sorted out for both a catcher gap and a velocity-filter gap by kinetic energy calculations.

Chapter V describes the effects of the second drift space and the velocity-filter gap on the characteristics of the spent beam. The analysis is similar to work in the previous chapters, the operating parameters for the catcher gap and the velocity-filter gap found in Chapter IV being used as initial conditions.

II. ANALYSIS OF THE FIRST GAP

The first or buncher gap modulates the velocity of an electron beam. This, in turn, causes density modulation in the drift space. In a finite gap, however, density modulation also takes place. This factor has been neglected in previous analyses, and including it here extends Webster's analysis.

Exact equations for the first gap will be derived from the equation of motion, and the characteristics of the beam will be calculated by the computer. Analytical expressions of functional relationships will be based on the exact graphic method with the assumptions mentioned. Thus in this chapter, a graphic analysis is first made, and then analytical formulas are obtained by successive approximations.

A. GRAPHIC ANALYSIS (Computer Problem)[3]

The equation of motion of electrons in the buncher gap, with a sinusoidal input voltage and no space charge, is a simple second-order differential equation,

$$\ddot{z} = \frac{eV_1}{md} \sin\omega t \quad . \tag{2.1}$$

Using the notation of Figure 1, integrating Equation (2.1) twice, and substituting boundary conditions at $t = t_a$ and at $t = t_b$, one obtains

$$\dot{z} = v_o + \frac{eV_1}{m\omega d} (\cos\omega t_a - \cos\omega t) \quad , \tag{2.2}$$

$$d = \left(v_o + \frac{eV_1}{m\omega d} \cos\omega t_a\right) (t_b - t_a) + \frac{eV_1}{m\omega^2 d} (\sin\omega t_a - \sin\omega t_b) \quad . \tag{2.3}$$

Defining the d-c transit angle and depth of modulation gives

$$\theta_g = \frac{\omega d}{v_o} \quad , \tag{2.4}$$

$$a = \frac{V_1}{V_o} \quad ; \tag{2.5}$$

and normalizing with respect to d-c velocity gives

$$\dot{Z} = \frac{\dot{z}}{v_o} = 1 + \frac{a}{2\theta_g} (\cos\omega t_a - \cos\omega t_b) \quad , \tag{2.6}$$

$$\theta_g = \left(1 + \frac{a}{2\theta_g} \cos\omega t_a\right)(\omega t_b - \omega t_a) + \frac{a}{2\theta_g} (\sin\omega t_a - \sin\omega t_b) \quad . \tag{2.7}$$

Equations (2.6) and (2.7) completely define the motion of electrons during the passage through the gap and give the implicit relation between entrance time and exit time with the gap transit angle and depth of modulation as parameters.

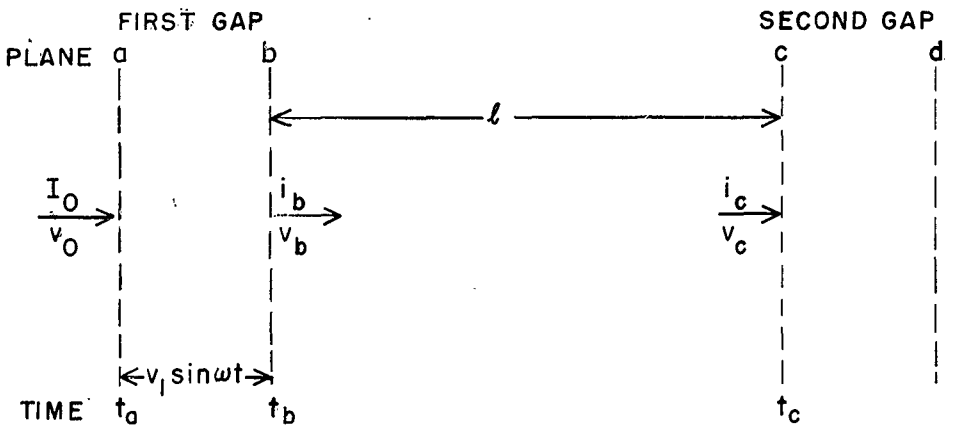

Figure 1. Schematic Diagram of Two-Cavity Klystron with Parallel Gridded Gaps.

The numerical computations of Equation (2.6) and (2.7) have been carried out on the digital computer and are presented in a series of graphs of normalized exit velocity, v_b/v_o, versus exit time, ωt_b; normalized exit current, i_b/I_o, versus exit time, ωt_b; and the transit-time correction factor, $\omega t_b - \omega t_a - \theta_g$, versus entrance time, ωt_a.

Exit current is obtained by applying the principle of conservation of charge through the gap; it can be determined from

$$\frac{i_b}{I_o} = \left| \frac{d\omega t_a}{d\omega t_b} \right| \quad . \tag{2.8}$$

Numerical values of the normalized current are found by measuring the slope of the curves of the transit-time correction factor versus entrance time at each point. Figures 2a, b, c show the results of this method for three different gap transit angles with depth of modulation as a parameter. Other results obtained by this method are presented in subsequent sections of this chapter.

It can be seen from Figures 2a, b, and c that the normalized exit current gradually becomes peaked as the d-c gap transit angle (θ_g) is increased, and that there is a phase difference between the normalized exit current and the normalized exit velocity. Since deceleration and acceleration of electrons during the corresponding half cycles of the input voltage counteract each other, there is a limit to this peaking of the exit current as the d-c gap transit angle is further increased; $\theta_g = \pi$ is a practical gap transit angle, and it is used in the computations throughout the rest of this chapter and in the next chapter.

The wave forms of the exit velocity and the exit current show that

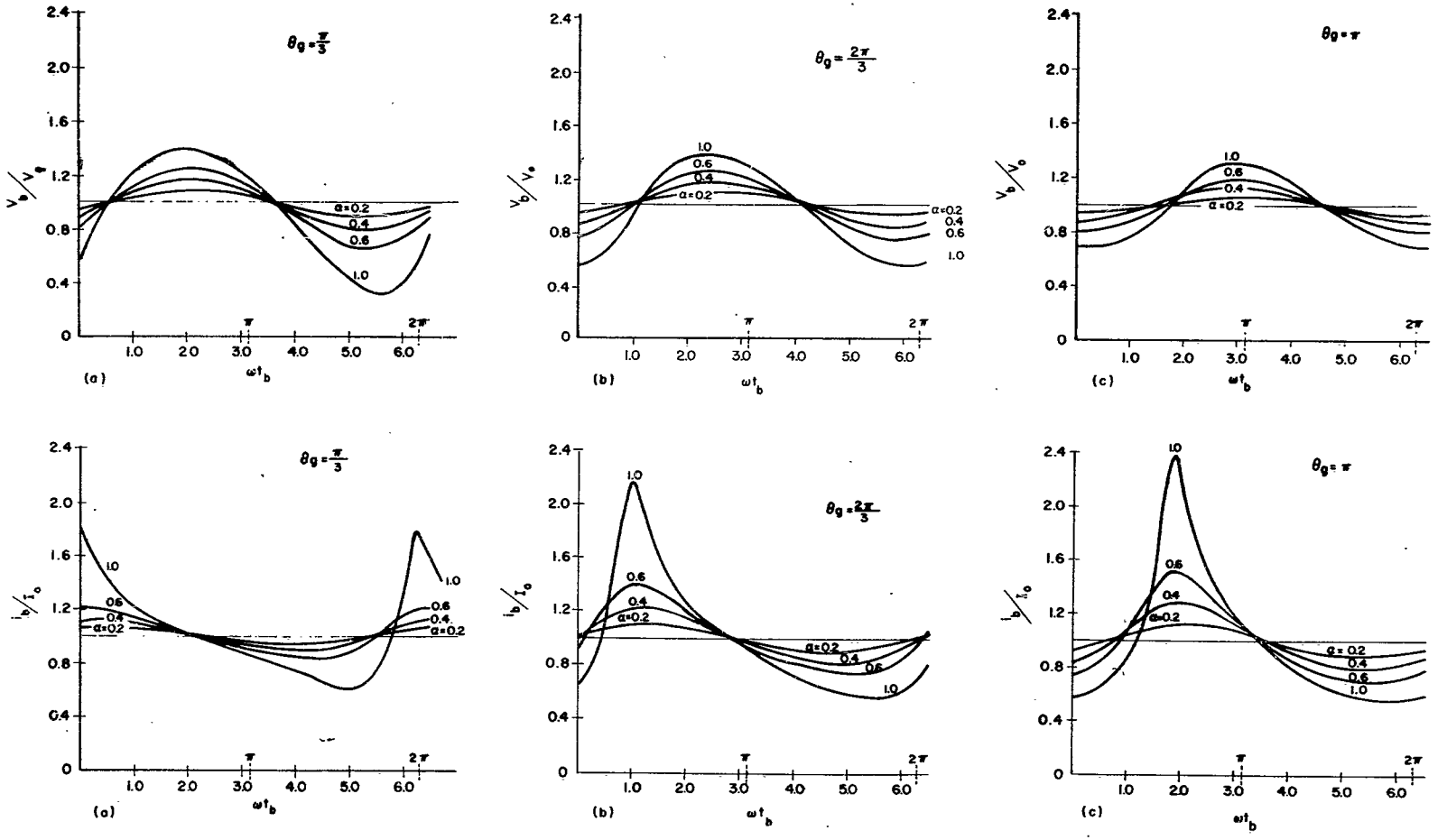

Figure 2. Normalized Exit Velocity v_b/v_o versus Exit Time ωt_b, and Normalized Exit Current i_b/I_o versus Exit Time ωt_b, for Different D-C Gap Transit Angles, Obtained by Graphic Analysis.

they both have harmonics and that transit-time effects are nonlinear in the buncher gap.

B. FIRST-ORDER ANALYSIS

When the results of graphic analysis are known, one can proceed with the analytical study by making approximations in the derivations, and comparing the results thus obtained with those of the exact graphic method. The discrepancies will show the validity and the range of the analytical forms.

1. Velocity Modulation

One must approximate the transit time, since it plays an important role in the physical phenomena within the buncher gap. Assuming a correction term,

$$\omega t_b = \omega t_a + \theta \quad , \tag{2.9}$$

where

$$\theta \doteq \theta_g(1 + \delta) \qquad \theta_g \delta = \omega t_b - \omega t_a - \theta_g \quad , \tag{2.10}$$

and substituting Equation (2.9) into Equation (2.2), one obtains for $t = t_b$,

$$\begin{aligned} v_b &= v_o + \frac{e}{m} \frac{V_1}{\omega d} \quad 2 \sin\frac{\theta}{2} \quad \sin\left(\omega t_b - \frac{\theta}{2}\right) \\ &= v_o + \frac{1}{2} v_o a \frac{\sin\frac{\theta}{2}}{\frac{\theta_g}{2}} \quad \sin\left(\omega t_b - \frac{\theta}{2}\right) \quad . \end{aligned} \tag{2.11}$$

Expanding $\sin(\omega t_b - \frac{\theta}{2})$ by trigonometric identities and neglecting δ terms of higher order than the linear term, one can write Equation (2.11) as

$$\frac{v_b}{v_o} = 1 + \frac{1}{2}\mu a \sin\left(\omega t_b - \frac{\theta_g}{2}\right) + \frac{1}{2} a\delta \cos\frac{\theta_g}{2} \sin\left(\omega t_b - \frac{\theta_g}{2}\right) - \frac{1}{4}\mu a\theta_g \cos\left(\omega t_b - \frac{\theta_g}{2}\right) , \tag{2.12}$$

where

$$\mu \equiv \sin\frac{\theta_g}{2} \Big/ \frac{\theta_g}{2} . \tag{2.13}$$

Integrating Equation (2.2) and substituting in it the boundary conditions at $t = t_a$ and at $t = t_b$, and Equation (2.9), one obtains

$$d = \frac{v_o\theta}{\omega} + \frac{a\theta v_o}{2\omega\theta_g} \cos(\omega t_b - \theta) + \frac{a v_o}{2\omega\theta_g} \left[\sin(\omega t_b - \theta) - \sin\omega t_b\right] . \tag{2.14}$$

Assuming

$$\cos\left[\omega t_b - \theta_g(1+\delta)\right] \approx \cos(\omega t_b - \theta_g) ,$$

$$\sin\left[\omega t_b - \theta_g(1+\delta)\right] \approx \sin(\omega t_b - \theta_g) ,$$

$$\therefore \sin\left[\omega t_b - \theta_g\delta\right] \approx \sin\omega t_b ,$$

and neglecting the $a\delta$ term gives

$$\delta = \frac{a}{2\theta_g^2} \left[A \sin\omega t_b + B\cos\omega t_b\right] , \tag{2.15}$$

where

$$A \equiv 1 - \cos\theta_g - \theta_g \sin\theta_g , \tag{2.16a}$$

$$B \equiv \sin\theta_g - \theta_g \cos\theta_g . \tag{2.16b}$$

Substitution of Equation (2.15) into Equation (2.12) leads to

$$\frac{v_b}{v_o} = 1 + \Delta + \frac{1}{2}\mu a \sin\left(\omega t_b - \frac{\theta_g}{2}\right) + M \sin 2\left(\omega t_b + \varphi\right) \quad , \qquad (2.17)$$

where

$$\Delta \equiv \frac{1}{2}\left(\frac{a}{2\theta_g}\right)^2 (\cos\theta_g - 1) \quad , \qquad (2.18a)$$

$$M \equiv \sqrt{P^2 + Q^2} \quad , \qquad (2.18b)$$

$$P \equiv \frac{1}{2}\left(\frac{a}{2\theta_g}\right)^2 (\sin 2\theta_g - \sin\theta_g - \theta_g + 2\theta_g \sin^2 \theta_g) \quad , \qquad (2.18c)$$

$$Q \equiv -\frac{1}{2}\left(\frac{a}{2\theta_g}\right)^2 \left(1 + \cos\theta_g - 2\cos^2 \theta_g - \theta_g \sin 2\theta_g\right) \quad , \qquad (2.18d)$$

$$2\varphi \equiv \tan^{-1}\frac{Q}{P} \quad . \qquad (2.18e)$$

Equation (2.15) is plotted in Figure 3 for $\theta_g = \pi$. It can be seen that while Equation (2.15) is a good approximation for small signals, it is a less satisfactory approximation for large signals.

2. Density Modulation

Substituting Equation (2.15) into Equation (2.10) and rewriting it, one obtains

$$\omega t_a = \omega t_b - \theta_g - \frac{a}{2\theta_g}\left[A \sin\omega t_b + B \cos\omega t_b\right] \quad . \qquad (2.19)$$

As in the graphic method, one can, by using Equation (2.8), express the normalized exit current as

$$\frac{i_b}{I_o} = 1 + \frac{a}{2\theta_g}(B \sin\omega t_b - A \cos\omega t_b) \quad . \qquad (2.20)$$

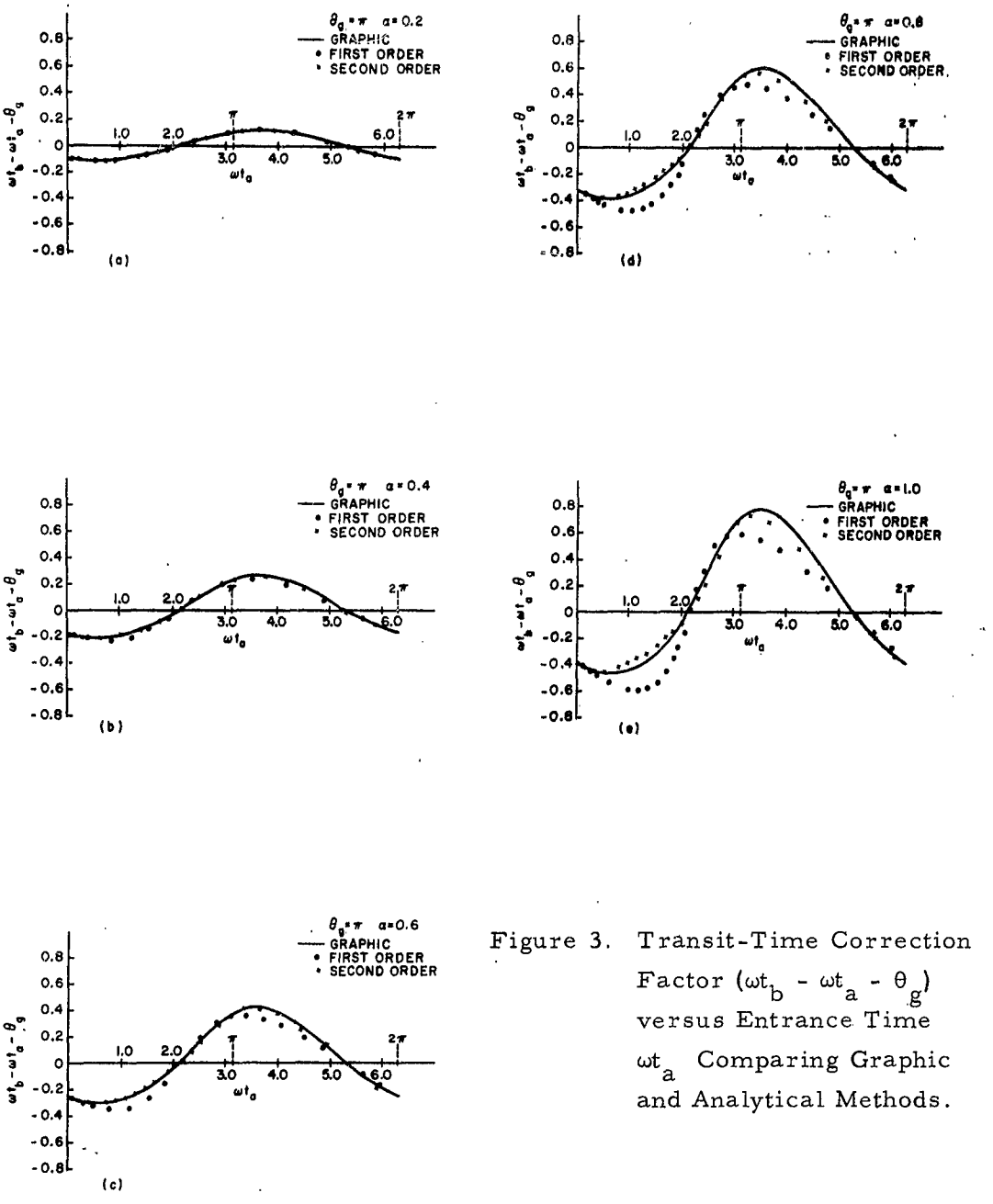

Figure 3. Transit-Time Correction Factor ($\omega t_b - \omega t_a - \theta_g$) versus Entrance Time ωt_a Comparing Graphic and Analytical Methods.

Equation (2.20) can also be written as

$$\frac{i_b}{I_o} = 1 + N \sin(\omega t_b + \psi) \quad , \tag{2.21}$$

where

$$N \equiv \frac{ac}{2\theta_g} \quad , \tag{2.22a}$$

$$C \equiv \sqrt{A^2 + B^2} \quad , \tag{2.22b}$$

$$\tan\psi \equiv \frac{-A}{B} \quad . \tag{2.22c}$$

From Figure 3 one can anticipate that Equation (2.21) will approach the results of the graphic method for small signals, but the discrepancy will be considerable for large signals.

It should be observed that the first-order analysis introduces a second-harmonic term into the velocity expression, while only the fundamental is involved in the current expression. One can conclude that the first-order analysis results in analytic forms that approximate those of the graphic method for the small-signal case, and that the method of approximation for the transit-time correction factor appears promising for the large-signal case. This approach will be followed, therefore, in the following analysis.

C. SECOND-ORDER ANALYSIS

Extending the transit-time correction-factor approximation one step further, assume that

$$\theta \equiv \theta_g(1 + \delta_1 + \delta_2) \quad , \tag{2.23}$$

where δ_1 is given by Equation (2.15). Substituting Equation (2.23) into Equation (2.14), assuming

$$\cos(\omega t_b - \theta) \approx \cos(\omega t_b - \theta_g - \theta_g\delta_1) + \theta_g\delta_2 \sin(\omega t_b - \theta_g - \theta_g\delta_1) \quad ,$$

$$\sin(\omega t_b - \theta) \approx \sin(\omega t_b - \theta_g - \theta_g\delta_1) - \theta_g\delta_2 \cos(\omega t_b - \theta_g - \theta_g\delta_1) \quad ,$$

and neglecting $a\delta_2$ and δ_2^2 terms, one obtains

$$\delta_2 = -\delta_1 + \frac{a}{2\theta_g^2}\left[\sin\omega t_b - \sin(\omega t_b - \theta_g - \theta_g\delta_1) - \theta_g(1+\delta_1)\cos(\omega t_b - \theta_g - \theta_g\delta_1)\right] \quad , \tag{2.24a}$$

and

$$\omega t_b - \omega t_a - \theta_g = \frac{a}{2\theta_g}\left[\sin\omega t_b - \sin(\omega t_b - \theta_g - \theta_g\delta_1) - \theta_g(1+\delta_1)\cos(\omega t_b - \theta_g - \theta_g\delta_1)\right] \quad . \tag{2.24b}$$

Equation (2.24b) is plotted in Figure 3 for $\theta_g = \pi$. It can be seen from this figure that Equation (2.24b) gives a fair approximation to the graphic results for larger signal values.

1. Velocity Modulation

Substitution of Equation (2.24a) into Equation (2.13) leads, after some rearrangement, to

$$\frac{v_b}{v_o} = 1 + \frac{1}{2}\left(\frac{a}{2\theta_g}\right)^2(\cos\theta_g - 1) - \frac{1}{4}\left(\frac{a}{2\theta_g}\right)^4\left[A^2 + B^2 - AB\sin 2\theta_g - \frac{B^2 - A^2}{2}\cos 2\theta_g\right]$$

$$+\left(\frac{a}{2\theta_g}\right)\left[\sin\theta_g - \frac{\theta_g}{4}\left(\frac{a}{2\theta_g}\right)^2 (2A + A\cos 2\theta_g - B\sin 2\theta_g)\right] \sin\omega t_b$$

$$-\left(\frac{a}{2\theta_g}\right)\left[1 - \cos\theta_g + \frac{\theta_g}{4}\left(\frac{a}{2\theta_g}\right)^2 (2B - A\sin 2\theta_g - B\cos 2\theta_g)\right] \cos\omega t_b$$

$$+\frac{1}{2}\left(\frac{a}{2\theta_g}\right)^2 B\left\{\cos\theta_g - A\sin\theta_g + \frac{1}{2}\left(\frac{a}{2\theta_g}\right)^2 \left[(A^2+B^2)\sin 2\theta_g - 2AB\right]\right\}\sin 2\omega t_b$$

$$-\frac{1}{2}\left(\frac{a}{2\theta_g}\right)^2 \left\{A\cos\theta_g + B\sin\theta_g - \frac{1}{2}\left(\frac{a}{2\theta_g}\right)^2 \left[(A^2+B^2)\cos 2\theta_g + A^2 - B^2\right]\right\}\cos 2\omega t_b$$

$$+\frac{\theta_g}{4}\left(\frac{a}{2\theta_g}\right)^3 (A\cos 2\theta_g + B\sin 2\theta_g)\sin 3\omega t_b$$

$$-\frac{\theta_g}{4}\left(\frac{a}{2\theta_g}\right)^3 (A\sin 2\theta_g - B\cos 2\theta_g)\cos 3\omega t_b + \frac{1}{8}\left(\frac{a}{2\theta_g}\right)^4 \left[(B^2 - A^2)\sin 2\theta_g\right.$$

$$\left. + 2AB\cos 2\theta_g\right]\sin 4\omega t_b + \frac{1}{8}\left(\frac{a}{2\theta_g}\right)^4 \left[(B^2 - A^2)\cos 2\theta_g - 2AB\sin 2\theta_g\right]\cos 4\omega t_b \ . \tag{2.25}$$

Equation (2.25) is plotted in Figure 4 for $\theta_g = \pi$ for comparison with the graphic method, and in Figures 5 and 6 with the d-c gap transit angle as a parameter. It can be seen from Figure 4 that Equation (2.25) approximates the graphic method fairly well up to large signals. Figures 5 and 6 show the effect of the d-c gap transit angle on the velocity modulation. As expected, it can be seen that the modulation effect decreases, because of partial cancellation, as the d-c gap transit angle is increased.

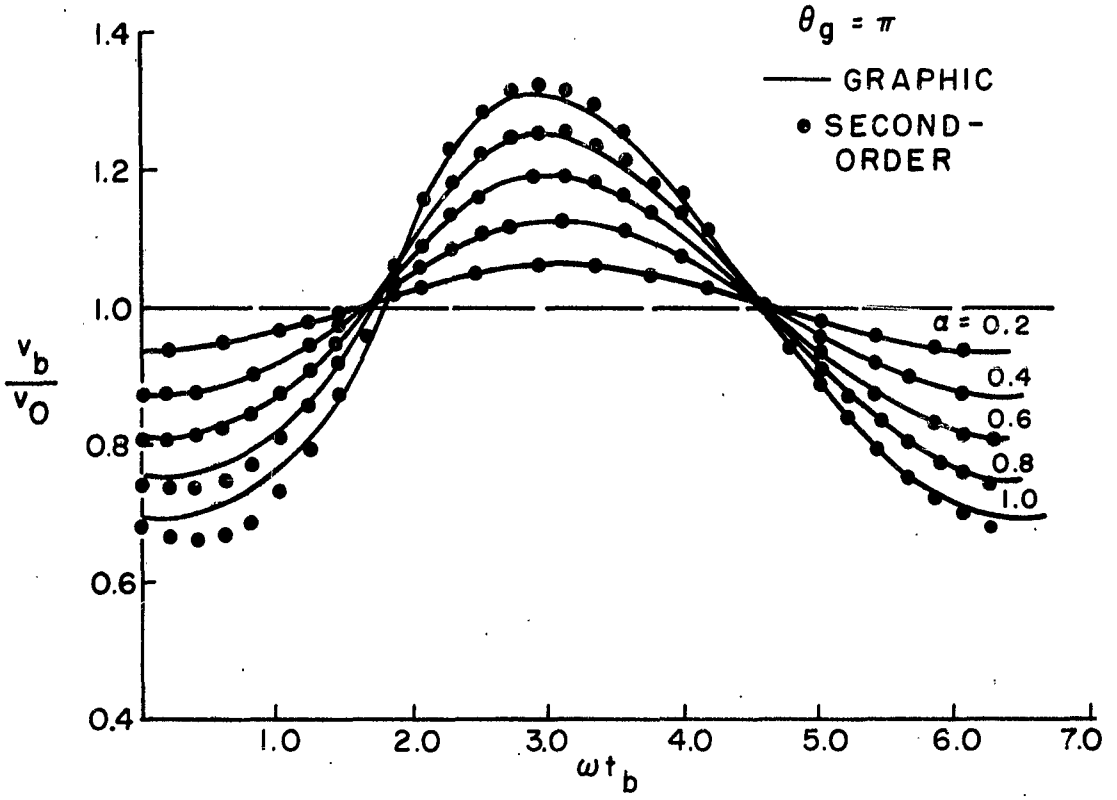

Figure 4. Normalized Exit Velocity v_b/v_o versus Exit Time ωt_b, Comparing Graphic and Second-Order Methods.

2. Density Modulation

Differentiating Equation (2.24b) and neglecting third-order terms, one obtains

$$\frac{i_b}{I_o} = \frac{d\omega t_a}{d\omega t_b} = 1 - \frac{\alpha}{2\theta_g}\left[\cos\omega t_b - \cos(\omega t_b - \theta_g) + \theta_g\left(1 - \theta_g\frac{d\delta_1}{d\omega t_b}\right.\right.$$

$$\left.\left. - \theta_g\delta_1\frac{d\delta_1}{d\omega t_b}\right)\sin(\omega t_b - \theta_g) - \theta_g^2\left(\delta_1 + \delta_1^2 - \theta_g\delta_1\frac{d\delta_1}{d\omega t_b}\right)\cos(\omega t_b - \theta_g)\right] . \quad (2.26)$$

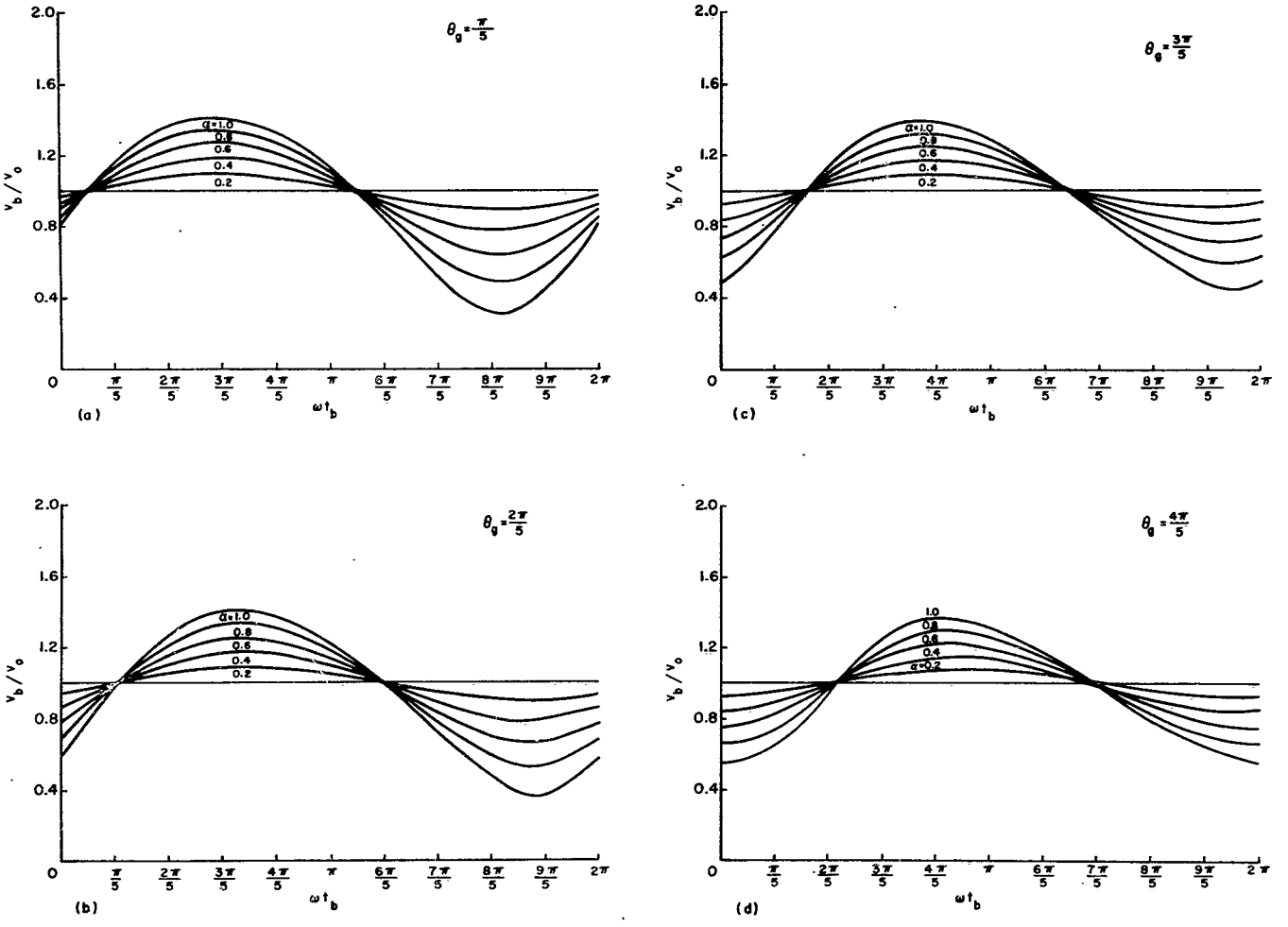

Figure 5. Normalized Exit Velocity v_b/v_o versus Exit Time. ωt_b for Different D-C Gap Transit Angles and Depths of Modulation.

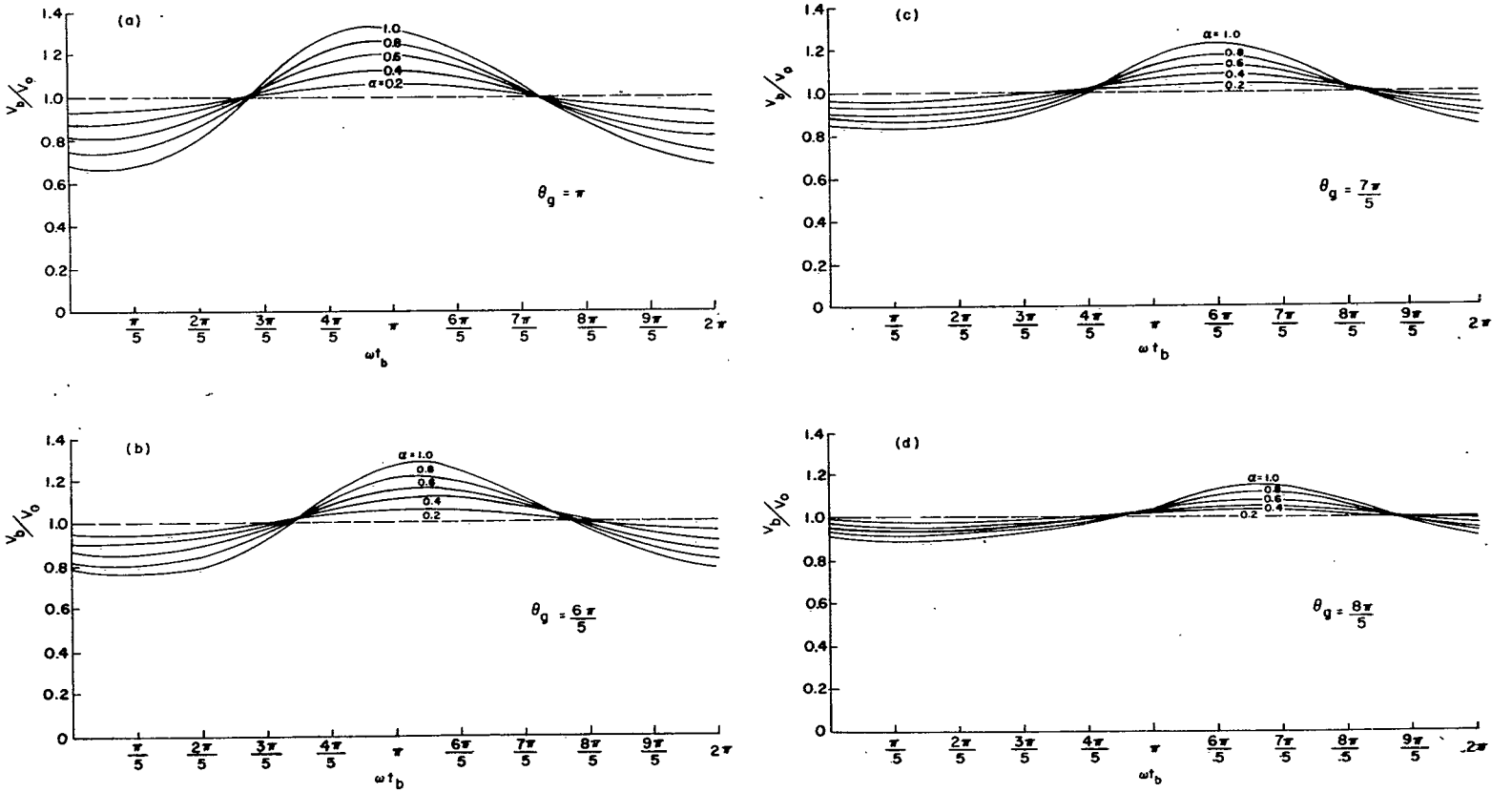

Figure 6. Normalized Exit Velocity v_b/v_o versus Exit Time ωt_b for Different D-C Gap Transit Angles and Depths of Modulation.

Substituting Equation (2.15) and its derivative with respect to ωt_b and rearranging terms gives

$$\frac{i_b}{I_o} = 1 + \left(\frac{a}{2\theta_g}\right)\left\{B + \frac{1}{2}\left(\frac{a}{2\theta_g}\right)^2\left[(A^2 + B^2 + \theta_g AB)\sin\theta_g - \frac{(A^2 - B^2)\,\theta_g}{2}\cos\theta_g\right]\right\}\sin\omega t_b$$

$$-\left(\frac{a}{2\theta_g}\right)\left\{A - \frac{1}{2}\left(\frac{a}{2\theta_g}\right)^2\left[(A^2 + B^2 - \theta_g AB)\cos\theta_g - \frac{(A^2 - B^2)}{2}\,\theta_g\sin\theta_g\right]\right\}\cos\omega t_b$$

$$+\left(\frac{a}{2\theta_g}\right)^2\theta_g(A\cos\theta_g + B\sin\theta_g)\sin 2\omega t_b - \left(\frac{a}{2\theta_g}\right)^2\theta_g(A\sin\theta_g - B\cos\theta_g)\cos 2\omega t_b$$

$$+\left(\frac{a}{2\theta_g}\right)^3\left[AB\cos\theta_g - \frac{(A^2 - B^2)}{4}\,\theta_g\cos\theta_g + \frac{(B^2 - A^2 - \theta_g AB)}{2}\sin\theta_g\right]\sin 3\omega t_b$$

$$-\left(\frac{a}{2\theta_g}\right)^3\left[AB\sin\theta_g - \frac{(A^2 - B^2)}{4}\,\theta_g\sin\theta_g - \frac{(B^2 - A^2 - \theta_g AB)}{2}\cos\theta_g\right]\cos 3\omega t_b \qquad (2.27)$$

Equation (2.27) is plotted in Figure 7 for $\theta_g = \pi$ for comparison with the graphic method, and in Figures 8 and 9 with the d-c gap transit angle as a parameter. Again it can be seen from Figure 7 that Equation (2.27) approximates the graphic method fairly well up to large signals. Figures 8 and 9 show the effect of the d-c gap transit angle on density modulation. As in the graphic method, it can be seen that density modulation first increases with the d-c gap transit angle and then decreases.

It should be observed that the second-order analysis introduces harmonics up to the third harmonic in the current expression, and up to

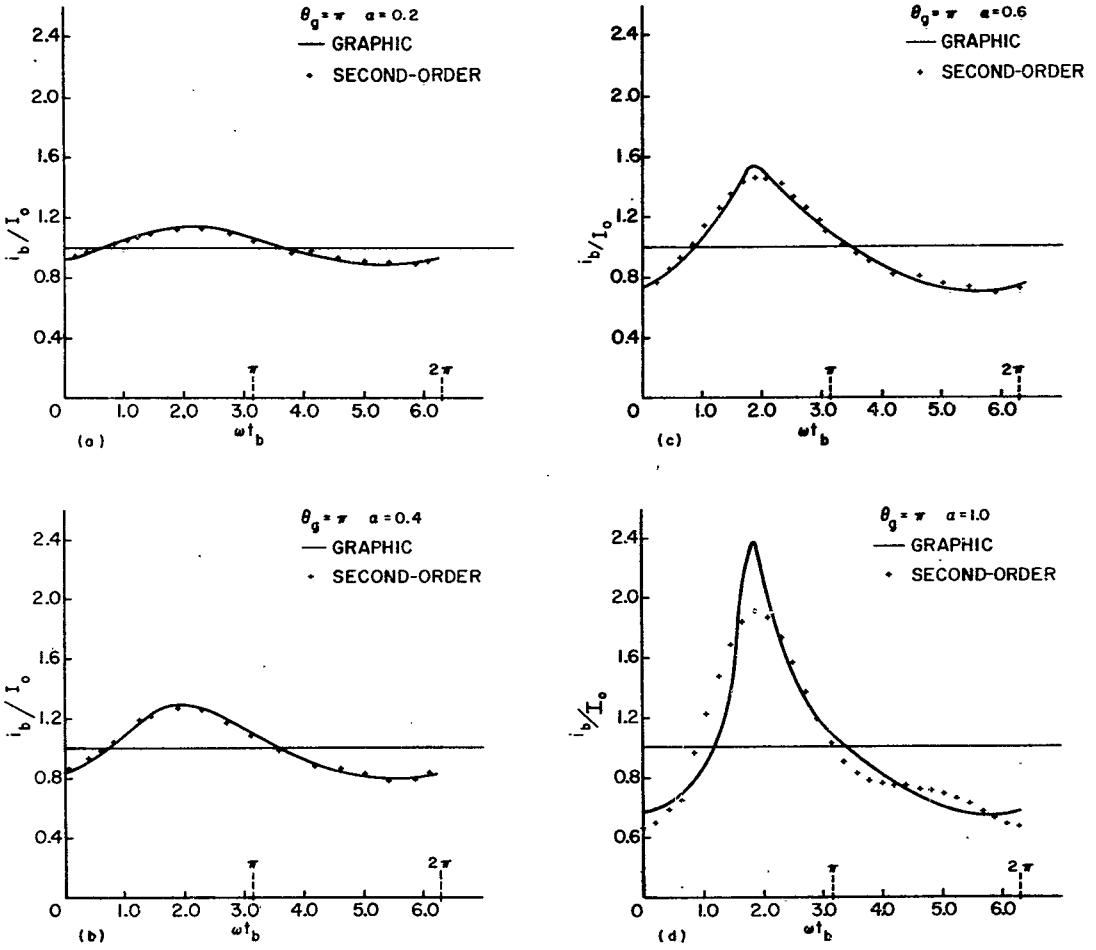

Figure 7. Normalized Exit Current i_b/I_o versus Exit Time ωt_b Comparing Graphic and Second-Order Methods.

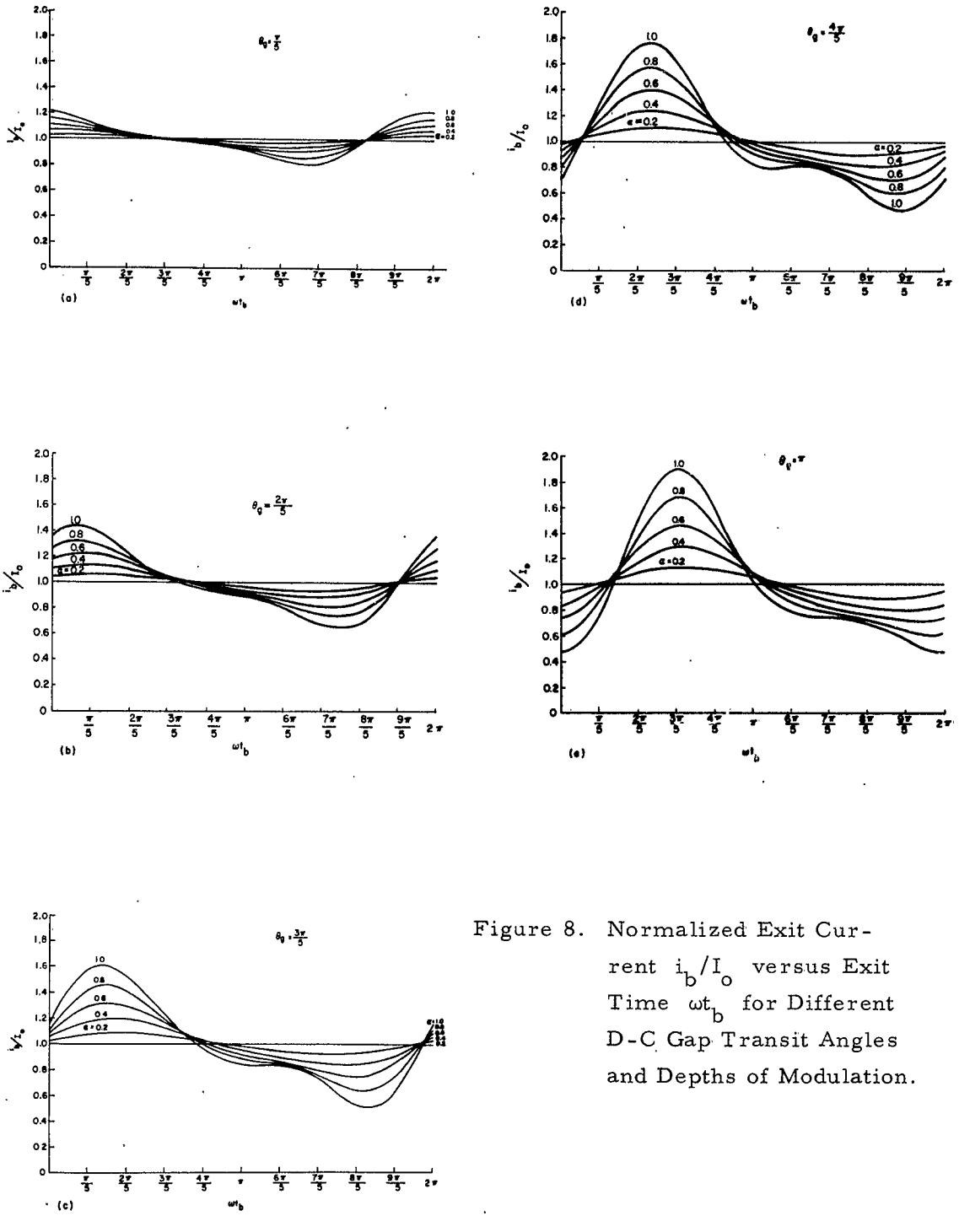

Figure 8. Normalized Exit Current i_b/I_o versus Exit Time ωt_b for Different D-C Gap Transit Angles and Depths of Modulation.

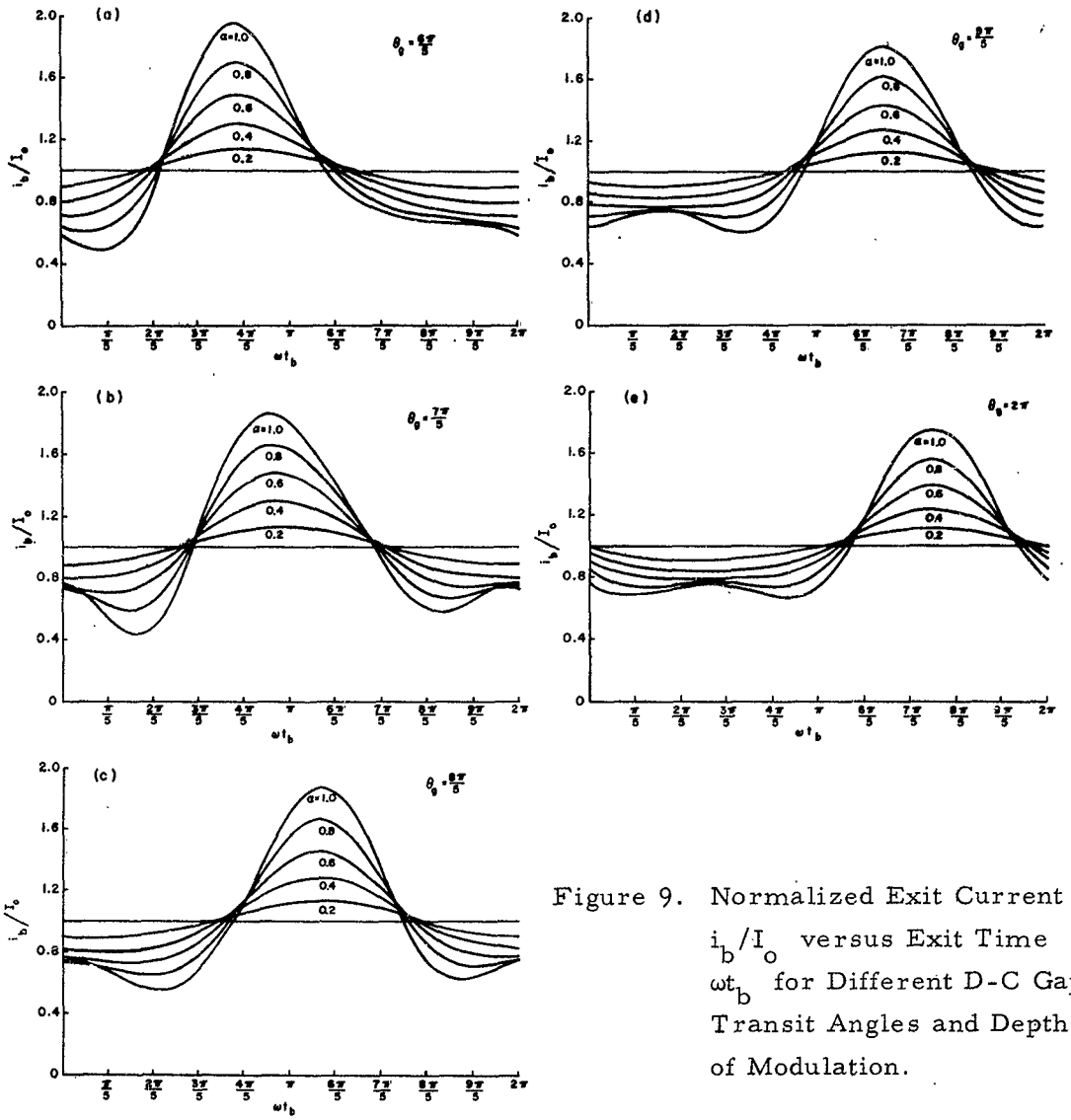

Figure 9. Normalized Exit Current i_b/I_o versus Exit Time ωt_b for Different D-C Gap Transit Angles and Depths of Modulation.

the fourth harmonic in the velocity expression, and that it extends the approximation to larger signals.

III. ANALYSIS OF THE FIRST DRIFT SPACE

The electron beam enters the drift space both velocity-modulated and density-modulated, and it drifts in a field-free space. This drift action produces further bunching of electrons, thereby increasing the harmonic content of the beam current. In his analysis, Webster neglects the density modulation produced in the gap, since his analysis deals with small signals. It was shown in the previous chapter that for large signals, the density modulation in the first gap was considerable, therefore the present analysis will consider the density modulation in the gap. It will include only first-order terms, however, and will not consider space-charge debunching. Although the present analysis is not valid after crossover, it will be extended beyond crossover; for qualitatively, it anticipates important trends.

The time at plane c (see Figure 1) can be expressed as

$$\omega t_c = \omega t_b + \frac{\omega l}{v_b} \quad . \tag{3.1}$$

Shifting the reference of time gives

$$\omega t_b' = \omega t_b - \frac{\theta_g}{2} \quad . \tag{3.2}$$

Dropping the prime, and neglecting the second-harmonic term in Equation (2.17), one obtains from Equation (3.1),

$$\omega t_c - \phi = \omega t_b - X \sin \omega t_b \quad , \tag{3.3}$$

where

$$\phi \equiv \theta_o (1 - \Delta) + \frac{\theta_g}{2} \quad , \tag{3.4a}$$

$$\theta_o \equiv \frac{\omega l}{v_o} \quad , \tag{3.4b}$$

$$X \equiv \frac{1}{2} \mu a \theta_o \quad . \tag{3.4c}$$

Equation (3.3) shows the functional relationship between the entrance and exit times of the drift space.

A. DENSITY

The principle of conservation of charge for the drift space states that

$$i_b \, d\omega t_b = i_c \, d\omega t_c \quad . \tag{3.5}$$

One can express the current at plane c as a Fourier series given by

$$i_c = A_o + \sum_{n=1}^{\infty} A_n \cos n(\omega t_c - \phi) + B_n \sin n(\omega t_c - \phi) \quad , \tag{3.6}$$

where

$$A_o = I_o \quad , \tag{3.7a}$$

$$A_n = \frac{1}{\pi} \int_o^{2\pi} i_c \cos n(\omega t_c - \phi) \, d\omega t_c \quad , \tag{3.7b}$$

$$B_n = \frac{1}{\pi} \int_o^{2\pi} i_c \sin n(\omega t_c - \phi) \, d\omega t_c \quad . \tag{3.7c}$$

If one uses Equations (2.20), (3.2), (3.3) and (3.5), then Equations (3.7b and c) become

$$A_n = \frac{I_o}{\pi} \int_0^{2\pi} \left[1 + N \sin\left(\omega t_b + \psi + \frac{\theta_g}{2}\right)\right] \cos n\left[\omega t_b - X \sin \omega t_b\right] d\omega t_b \quad , \quad (3.8a)$$

$$B_n = \frac{I_o}{\pi} \int_0^{2\pi} \left[1 + N \sin\left(\omega t_b + \psi + \frac{\theta_g}{2}\right)\right] \sin n\left[\omega t_b - X \sin \omega t_b\right] d\omega t_b \quad . \quad (3.8b)$$

Using Bessel function expressions[4] for trigonometric functions, integrating, and using recursion formulas for Bessel functions, one obtains

$$\frac{i_c}{I_o} = 1 + 2\left[1 + \frac{N}{X} \sin\left(\psi + \frac{\theta_g}{2}\right)\right] \sum_{n=1}^{\infty} J_n(nX) \cos n(\omega t_c - \phi) \quad ,$$

$$+ 2N \cos\left(\psi + \frac{\theta_g}{2}\right) \sum_{n=1}^{\infty} \frac{J_n'(nX)}{n} \sin n(\omega t_c - \phi) \quad . \quad (3.9)$$

It can be seen from Equation (3.9) that the beam current at plane c is rich in harmonics and that each harmonic can be calculated for any specified condition from the equation. Equation (3.9) reduces to that of Webster for small signals. It should also be noted that an additional phase angle, β_n, is introduced by the two independent components of each harmonic, given by

$$\tan \beta_n = \frac{\left[1 + \frac{N}{X} \sin\left(\psi + \frac{\theta_g}{2}\right)\right] n J_n(nX)}{N \cos\left(\psi + \frac{\theta_g}{2}\right) J_n'(nX)} \quad . \quad (3.10)$$

Figures 10a, 11a, and 12a show the first three harmonics, and Figures 10b, 11b, and 12b show the phase angles of these harmonics as a function of the bunching parameter (X), with the depth of modulation as a parameter, for $\theta_g = \pi$. The maximum amplitudes of the fundamental current for different depths of modulation (see Figure 10a) are seen to be greater than the usual value of 1.16, which was also predicted in a ballistic analysis by Webber[5] that included space-charge effects.

The first three harmonics are also plotted in Figure 13 as functions of the drift angle θ_o for $\theta_g = \pi$. Qualitatively Figure 13a resembles the experimental curves of Mihran, who also observed a saturation of the maxima of the fundamental current, although he did not explain the resaon for this.

Although space-charge effects were neglected in this study, the results obtained parallel those of others within the range of validity. A comparison with Solymar's[6] results is shown in Figure 14, where it was assumed that

$$\beta_p Z = \frac{\theta_o}{k} \quad . \tag{3.11}$$

B. VELOCITY

The transit time through the drift space can be assumed to be

$$\omega t_b - (\omega t_c - \phi) = \sum_{l=1}^{\infty} b_l \sin l(\omega t_c - \phi) \quad , \tag{3.12}$$

where

$$b_l = \frac{1}{\pi} \int_{-\pi}^{\pi} \left[\omega t_b - (\omega t_c - \phi)\right] \sin l(\omega t_c - \phi)\, d(\omega t_c - \phi) \quad . \tag{3.13}$$

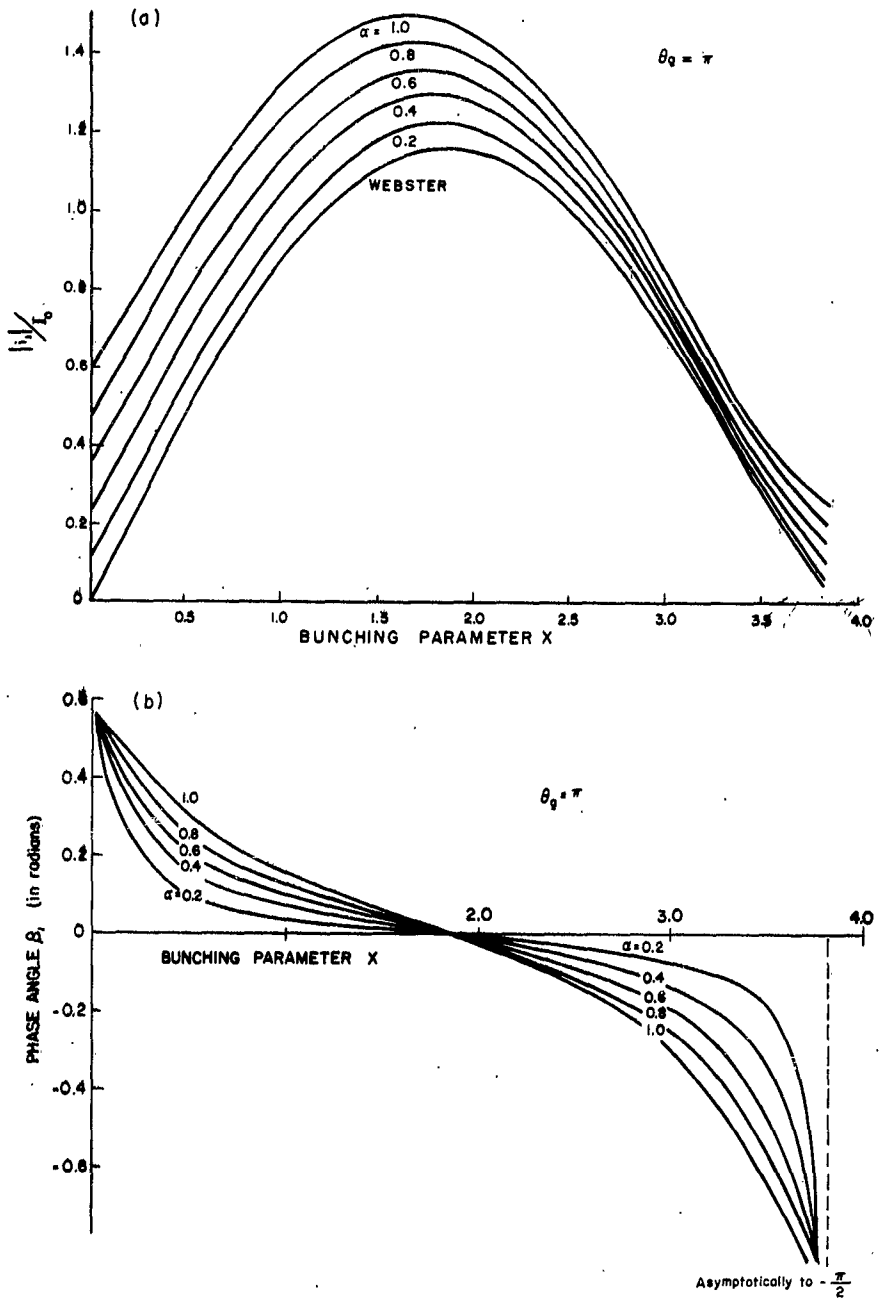

Figure 10. (a) Absolute Value of Normalized Fundamental Current $|i_1|/I_o$ versus Bunching Parameter X, (b) Phase Angle, β, versus Bunching Parameter X.

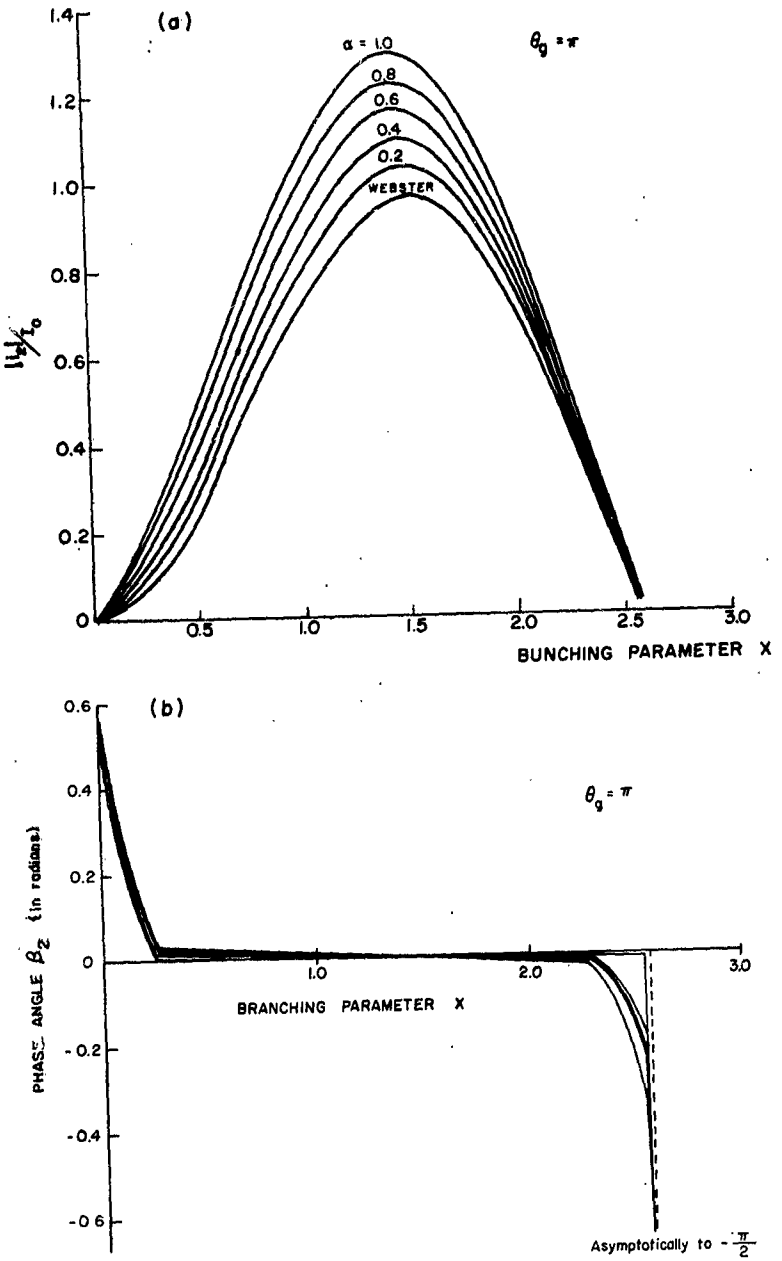

Figure 11. (a) Absolute Value of Normalized Second-Harmonic Current $|i_2|/I_o$ versus Bunching Parameter X , (b) Phase Angle β_2 versus Bunching Parameter X , in Drift Space.

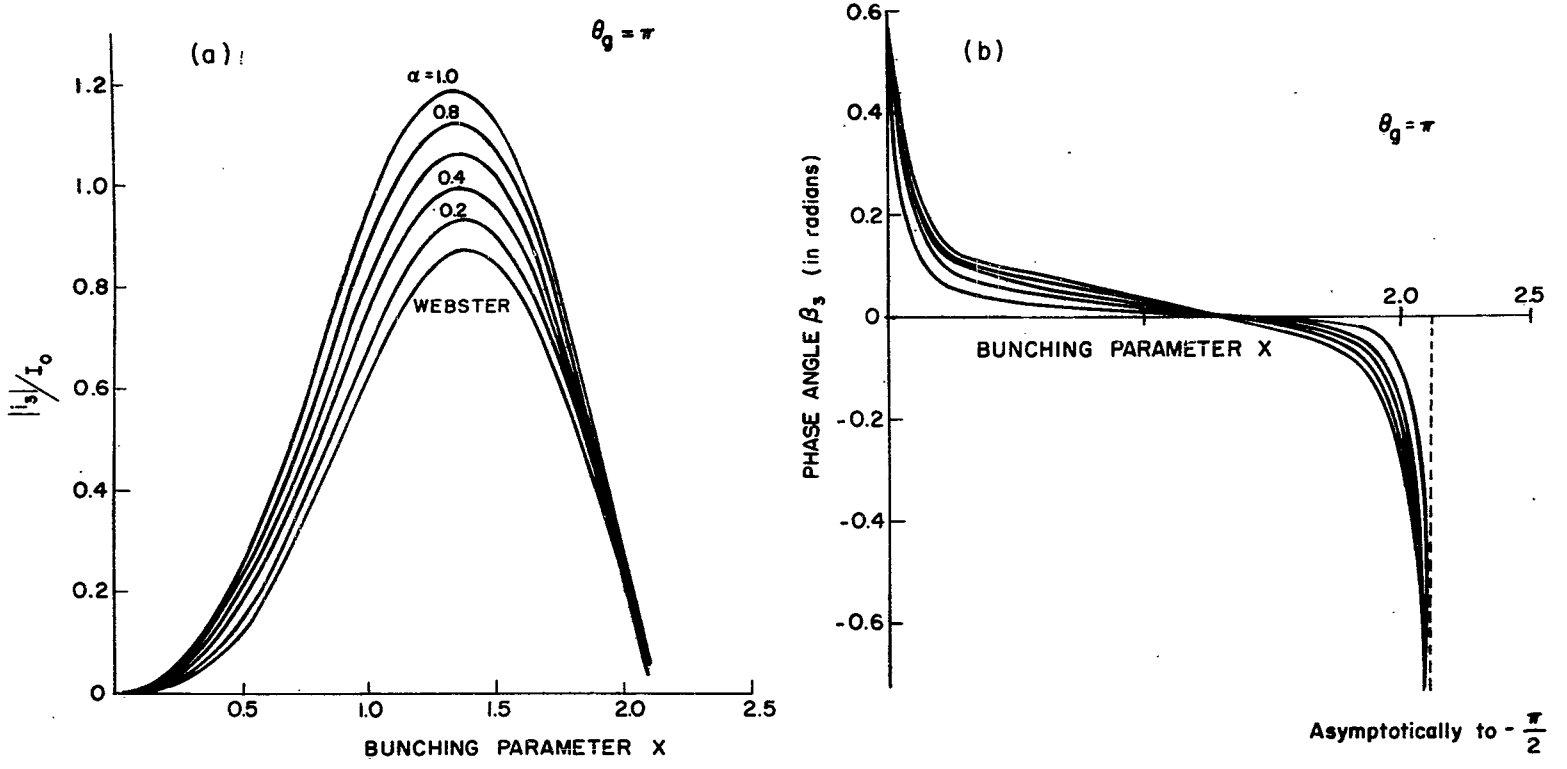

Figure 12. (a) Absolute Value of Normalized Third-Harmonic Current $|i_3|/I_o$ versus Bunching Parameter X, (b) Phase Angle β_3 versus Bunching Parameter X in the Drift Space.

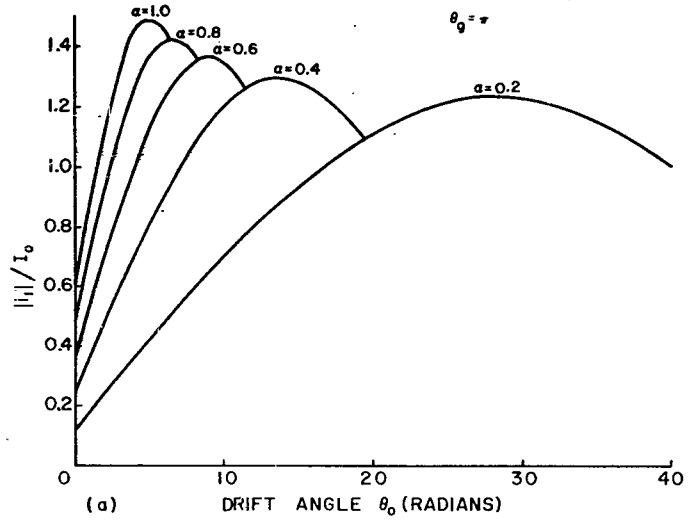

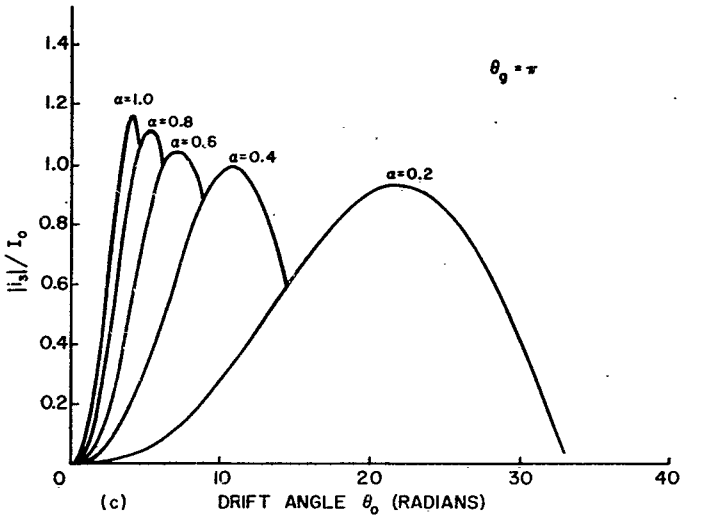

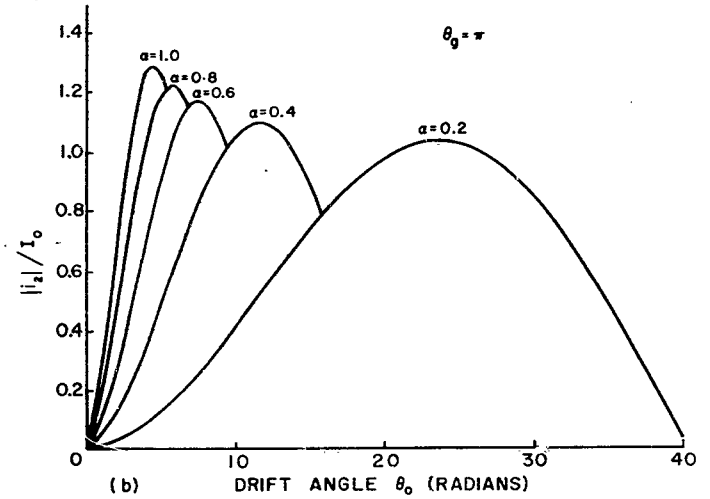

Figure 13. Absolute Value of Normalized Components of Current versus Drift Angle for Different Depths of Modulation.

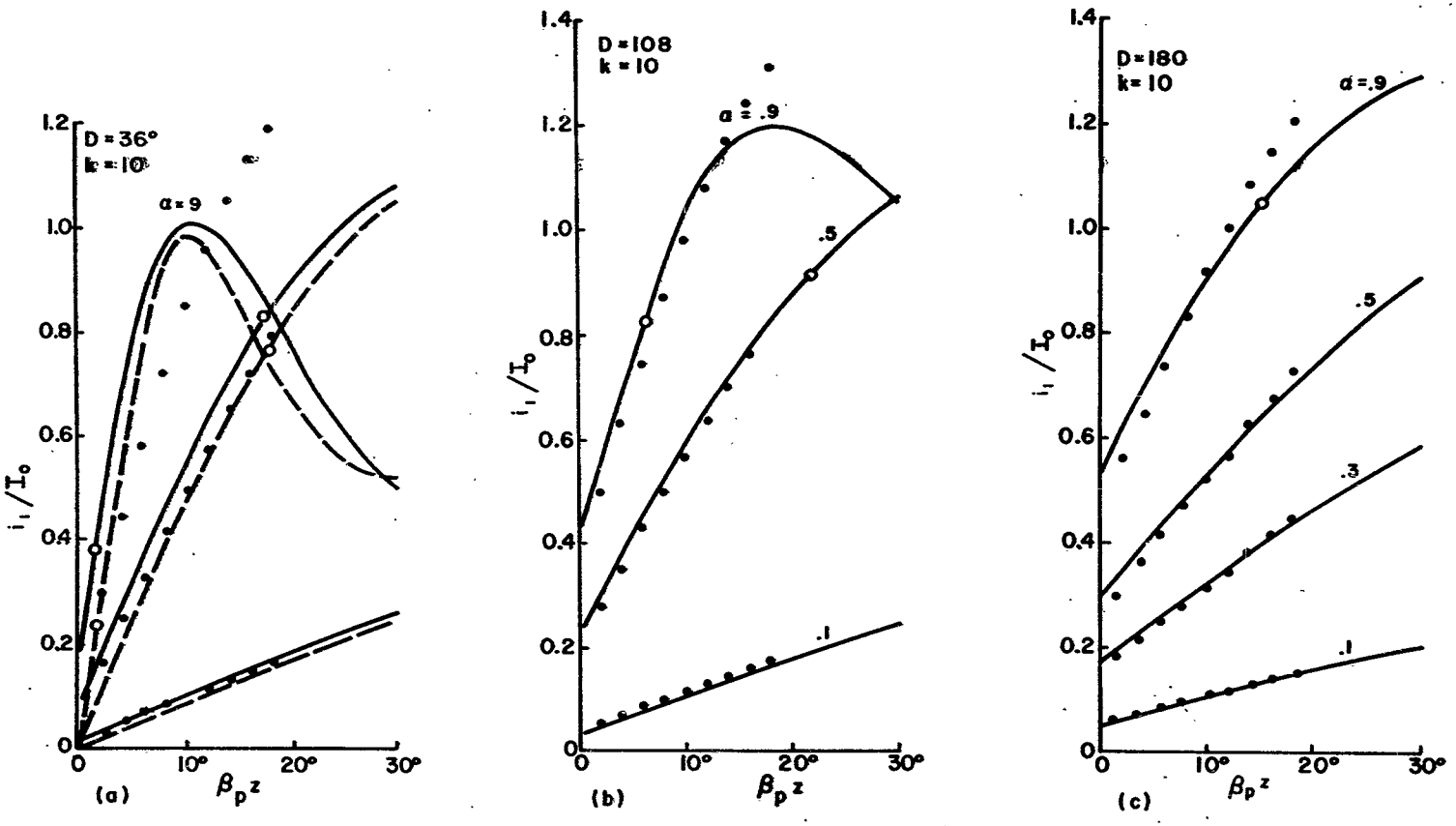

Figure 14. Normalized Fundamental Current i_1/I_o versus Normalized Drift Distance $\beta_p z$ for Different D-C Gap Transit Angles. (The curves shown are those calculated by Solymar. The solid dots are the points calculated from Equation (3.9) of this study.)

Integrating Equation (3.13) by parts and substituting Equation (3.3), one obtains

$$\omega t_b = \omega t_c - \phi + \sum_{l=1}^{\infty} \frac{2}{l} J_l(lX) \sin l(\omega t_c - \phi) \quad . \qquad (3.14)$$

Equation (3.14) shows the functional relationship between the entrance time and the exit time of the drift space. Figure 15 shows a comparison of Equation (3.3) and (3.14), where only the first three harmonics are included in Equation (3.14).

Since the drift space is assumed to be field-free, the equation of motion becomes

$$\ddot{z} = 0 \quad . \qquad (3.15)$$

Integrating Equation (3.15) and applying the boundary conditions at $t = t_b$, substituting Equation (2.17) with second harmonic terms neglected and Equations (3.2) and (3.14), one obtains

$$\frac{v_c}{v_o} = 1 + \Delta + \frac{1}{2} \mu a \sin \left[(\omega t_c - \phi) + \sum_{l=1}^{\infty} \frac{2J_l(lX)}{l} \sin l(\omega t_c - \phi) \right] \quad . \qquad (3.16)$$

Equation (3.16) is plotted in Figure 16 with depth of modulation as a parameter for $\theta_g = \pi$ and $\theta_o = \pi/2$.

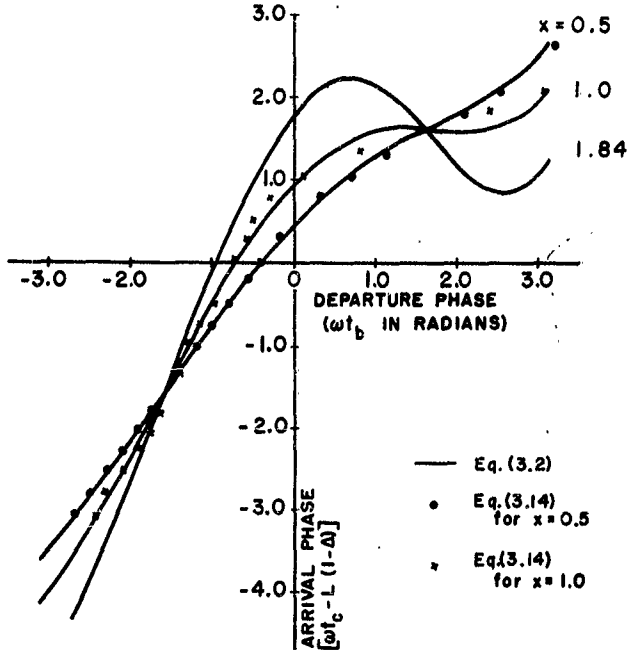

Figure 15. Arrival Phase, $\omega t_c - L(1 - \Delta)$, versus Departure Phase ωt_b for the Drift Space for Different Bunching Parameters.

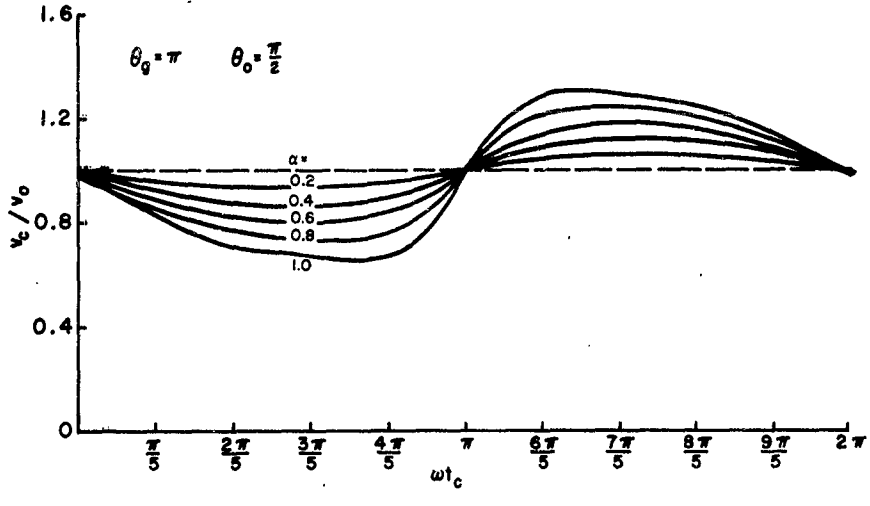

Figure 16. Normalized Exit Velocity v_c/v_o versus Exit Time ωt_c at End of Drift Space for Different Depths of Modulation.

IV. ANALYSIS OF THE SECOND GAP

It is well known that an electron beam has nonlinear characteristics and is rich in harmonics at the end of a klystron drift space. Analysis of the beam through a second gap, therefore, becomes complicated, because of overtaking and the multivalued nature of transit times. Analytical formulas, which can be derived from such an analysis by making approximations similar to those made in Chapter II, become implicit expressions of entrance and exit times as well as of various operating parameters.

For these reasons, only computer solutions are obtained in the remaining parts of this study. Thus the main effort will be directed to computing velocities and currents of a spent beam as functions of time rather than formulating them analytically. This will permit realization of the purpose of this study: (1) to investigate the characteristics of a spent beam in a two-cavity klystron and (2) to investigate the velocity-filtering capabilities of a r-f gap, using these characteristics as initial conditions. Additional information will be obtained about power output and tuning conditions of the catcher gap of a two-cavity klystron for optimum operation, since both velocities and currents will be known at the entrance to and at the exit of the second gap. Numerical calculations of kinetic energy will suffice for this purpose.

A. COMPUTER PROBLEM

Fundamental current at the entrance to the second gap can be expressed, by combining its two components, (see Equations 3.9 and 3.10), as

$$i_{c_1} = k \sin(\omega t - \phi + \beta_1) \quad , \tag{4.1}$$

where k is the amplitude of the fundamental. Assuming a voltage V_2 across the second gap with a phase angle Γ_2 with respect to fundamental current, one can write the equation of motion for this gap as

$$\ddot{z} = -\frac{e}{m} \frac{V_2}{d} \sin(\omega t + \xi) \quad , \tag{4.2}$$

where

$$\xi = -\phi + \beta_1 + \Gamma_2 \quad . \tag{4.3}$$

Integrating Equation (4.2) twice, substituting initial conditions at $t = t_c$, and normalizing with respect to d-c velocity, one obtains

$$\dot{Z} = \frac{v_c}{v_o} + \frac{a_2}{2\theta_{g_2}} \left[\cos(\omega t + \xi) - \cos(\omega t_c + \xi)\right] \quad , \tag{4.4}$$

$$Z = \left[\frac{v_c}{v_o} - \frac{a_2}{2\theta_{g_2}} \cos(\omega t_c + \xi)\right] (t - t_c) + \frac{a_2}{2\omega\theta_{g_2}} \left[\sin(\omega t + \xi) - \sin(\omega t_c + \xi)\right] \quad , \tag{4.5}$$

where a_2 is the ratio of the assumed voltage V_2 to the d-c beam voltage V_o, and where the d-c gap transit angle, θ_{g_2}, is defined by

$$\theta_{g_2} \equiv \frac{\omega d_2}{v_o} \quad . \tag{4.6}$$

Applying boundary conditions at $t = t_d$ to Equations (4.4) and (4.5) and multiplying Equation (4.5) by ω gives the following equations:

$$\theta_{g_2} = \left[\frac{v_c}{v_o} - \frac{a_2}{2\theta_{g_2}} \cos(\omega t_c + \xi)\right] (\omega t_d - \omega t_c) + \frac{a_2}{2\theta_{g_2}} \left[\sin(\omega t + \xi) - \sin(\omega t_c + \xi)\right] , \tag{4.7}$$

$$\frac{v_d}{v_o} = \frac{v_c}{v_o} + \frac{a_2}{2\theta_{g_2}} \left[\cos(\omega t_d + \xi) - \cos(\omega t_c + \xi)\right] . \tag{4.8}$$

Equation (4.7) is used to compute the exit time ωt_d, and Equation (4.8) to compute the normalized exit velocity v_d/v_o for a given entrance time ωt_c and for different gap parameters of a_2, θ_{g_2}, and Γ_2.

The normalized exit current is found by using the principle of conservation of charge, and is expressed as,

$$\frac{i_d}{I_o} = \frac{\frac{i_c}{I_o}}{\left|\frac{d\omega t_d}{d\omega t_c}\right|} . \tag{4.9}$$

The denominator of Equation (4.9) is derived by differentiating Equation (4.7) with respect to ωt_c, and it is given by

$$\frac{d\omega t_d}{d\omega t_c} = \frac{\frac{v_c}{v_o} - \frac{a_2}{2\theta_{g_2}} (\omega t_d - \omega t_c) \sin(\omega t_c + \xi) - (\omega t_d - \omega t_c) \frac{d}{d\omega t_c}\left(\frac{v_c}{v_o}\right)}{\frac{v_c}{v_o} + \frac{a_2}{2\theta_{g_2}} \left[\cos(\omega t_d + \xi) - \cos(\omega t_c + \xi)\right]} . \tag{4.10}$$

It should be noted that the normalized entrance velocity v_c/v_o given by Equation (3.16) is a single-valued function of ωt_c and cannot be used for

large signals. On the other hand, the normalized entrance current i_c/I_o, given in series form by Equation (3.9), is not suitable for a computer.

In the first drift space one has

$$i_b \, d\,\omega t_b = i_c \, d\,\omega t_c \quad , \tag{3.5}$$

$$\ddot{z} = 0 \quad , \tag{3.15}$$

$$\frac{i_b}{I_o} = 1 + N \sin(\omega t_b + \psi) \quad , \tag{2.21}$$

$$\frac{v_b}{v_o} = 1 + \Delta + \frac{1}{2}\mu a \sin\left(\omega t_b - \frac{\theta_g}{2}\right) + M \sin 2(\omega t_b + \psi) \quad . \tag{2.17}$$

Defining

$$x_k = \omega t_b - \frac{\theta_g}{2} \tag{4.11}$$

and neglecting the second-harmonic term in Equation (2.17), one can derive the following formulas, which take the multivaluedness into account, and which can be used in a computer:

$$\omega t_c = x_k + \frac{\theta_{o1}}{1 + \Delta + \frac{1}{2}\mu a \sin x_k} \quad , \tag{4.12}$$

$$\Delta t_k = \frac{d\omega t_c}{d x_k} = 1 - \frac{\frac{1}{2}\theta_{o1}\mu a \cos x_k}{\left(1 + \Delta + \frac{1}{2}\mu a \sin x_k\right)^2} \quad , \tag{4.13}$$

$$\frac{i_c}{I_o} = \sum_k \frac{1 + N \sin(x_k + \psi + \theta_{g/2})}{|\Delta t_k|} \quad , \tag{4.14}$$

$$\frac{v_c}{v_o} = 1 + \Delta + \frac{1}{2}\mu a \sin x_k \quad , \tag{4.15}$$

$$\frac{d}{d\omega t_c}\left(\frac{v_c}{v_o}\right) = \frac{\frac{1}{2}\mu a \cos x_k}{\Delta t_k} \quad . \tag{4.16}$$

Equation (4.14) gives the sum of the series in Equation (3.9) and is easily applicable to computer programming. Equation (4.15) is likewise multi-valued and can therefore also be used for large signals.

It should be noted that Equation (4.9) does not contain the summation sign; therefore it gives the component of the normalized exit current i_d/I_o which corresponds to an increment of a specific entrance time ωt_c. The intention here is to follow the separate current contributions from the increments of different entrance time ωt_c in future computations. This point will be discussed again in later sections.

B. CALCULATION OF KINETIC ENERGY AND DISCUSSION

Equations (4.7) – (4.9) with the auxiliary Equations, (4.10) and (4.12) – (4.16) were computed by the digital computer. In order to allow experimental verification of the results obtained from the computer, the physical magnitudes of the input parameters were selected to be applicable to the dynamic beam analyzer,[7] which is an experimental tool available in this laboratory. Therefore a value of 1.75 radians for the d-c transit angle of the first gap θ_g and a value of 2π radians for the normalized drift distance θ_o were chosen. This value of θ_o places the second gap at about one-eighth of a space-charge wavelength of the dynamic beam tester.

The depths of modulation in the first gap a_1 and the second gap, a_2, are taken from 0.2 to 1.0 in 0.2 steps; the d-c gap transit angle of the second gap θ_{g_2} was taken from $\pi/4$ to 2π radians in $\pi/4$-radian steps; and finally the phase angle Γ_2 of the assumed voltage V_2 across the second gap with respect to the fundamental current at the entrance was taken from $-\pi$ to π radians in $\pi/4$-radian steps. For all cases mentioned above, the entrance time ωt_c was changed from 0 to 2π radians with different increments chosen from the curves of the normalized entrance current i_c/I_o versus entrance time ωt_c as needed. Thus, it can be seen that the computer calculations cover a wide range of operating conditions.

It should be pointed out here that the assumed voltage V_2 across the second gap may either be induced by the electron beam or be applied externally. Separation of these states is possible by kinetic energy calculations at the entrance to the second gap and at the exit from it. Obviously, a decrease in kinetic energy through the second gap indicates that power is taken out and that the voltage V_2 is induced by the electron beam. An increase in kinetic energy, on the other hand, signifies that power is fed into the second gap and hence that voltage V_2 is applied externally. The argument for the existence of such a gap voltage depends upon the physical realizability of the circuit parameters associated with its phase angle Γ_2, i.e., actual total admittance and resonant frequency of a specific cavity used as the second gap. This point will be discussed further in the next section.

The computer data are so arranged that, for a given set of operating parameters, the normalized exit current i_d/I_o, the normalized exit velocity v_d/v_o, and the exit time ωt_d are given, together with their corre-

sponding counterparts at the entrance; i.e., the normalized entrance current i_c/I_o, the normalized entrance velocity v_c/v_o, and the entrance time ωt_c.

Normalized kinetic energy per cycle of the electron beam can be computed from

$$2\pi W = \frac{W_k}{I_o V_o} = \int_o^{2\pi} \left(\frac{i}{I_o}\right)\left(\frac{v}{v_o}\right)^2 \, d\omega t \quad , \tag{4.17}$$

where W_k is the kinetic energy per cycle, i/I_o is the normalized current, and v/v_o is the normalized velocity at time ωt.

1. Two-Cavity Klystron and Velocity-Filter Gap

Figure 17 shows the fundamental component of beam current at the entrance to the second gap for different depths of modulation α_1 at the first gap with a value of 1.75 radians for the d-c transit angle of the first gap θ_g as a function of the first drift angle θ_o. The drift angle of 2π radians used in the computer run is shown by a vertical dashed line. It is seen from the figure that the maximum value of the fundamental current occurs between $\alpha_1 = 0.6$ and $\alpha_1 = 0.8$.

Figure 18 shows the normalized current i_c/I_o and the normalized velocity v_c/v_o at the entrance to the second gap for different depths of modulation α_1 at the first gap. Velocity curves in Figure 18 indicate that there are two stationary points on all curves. These points correspond to those electrons that pass through the first gap at times when the r-f field at the first gap changes from decelerating to accelerating and vice versa. With respect to the stationary points, therefore, electrons in the beam at

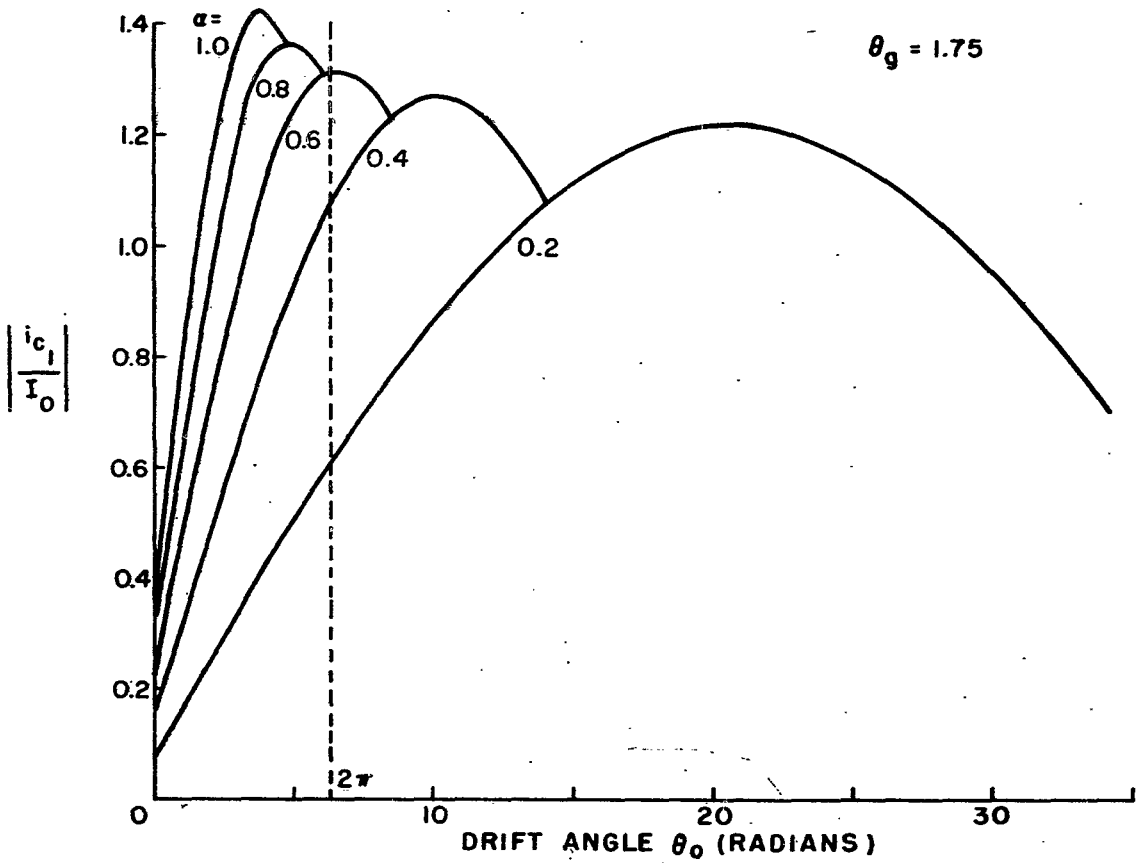

Figure 17. Absolute Value of Normalized Fundamental Current $|i_{c_1}/I_o|$ versus Drift Angle θ_o at Entrance to Second Gap for Different Depths of Modulation.

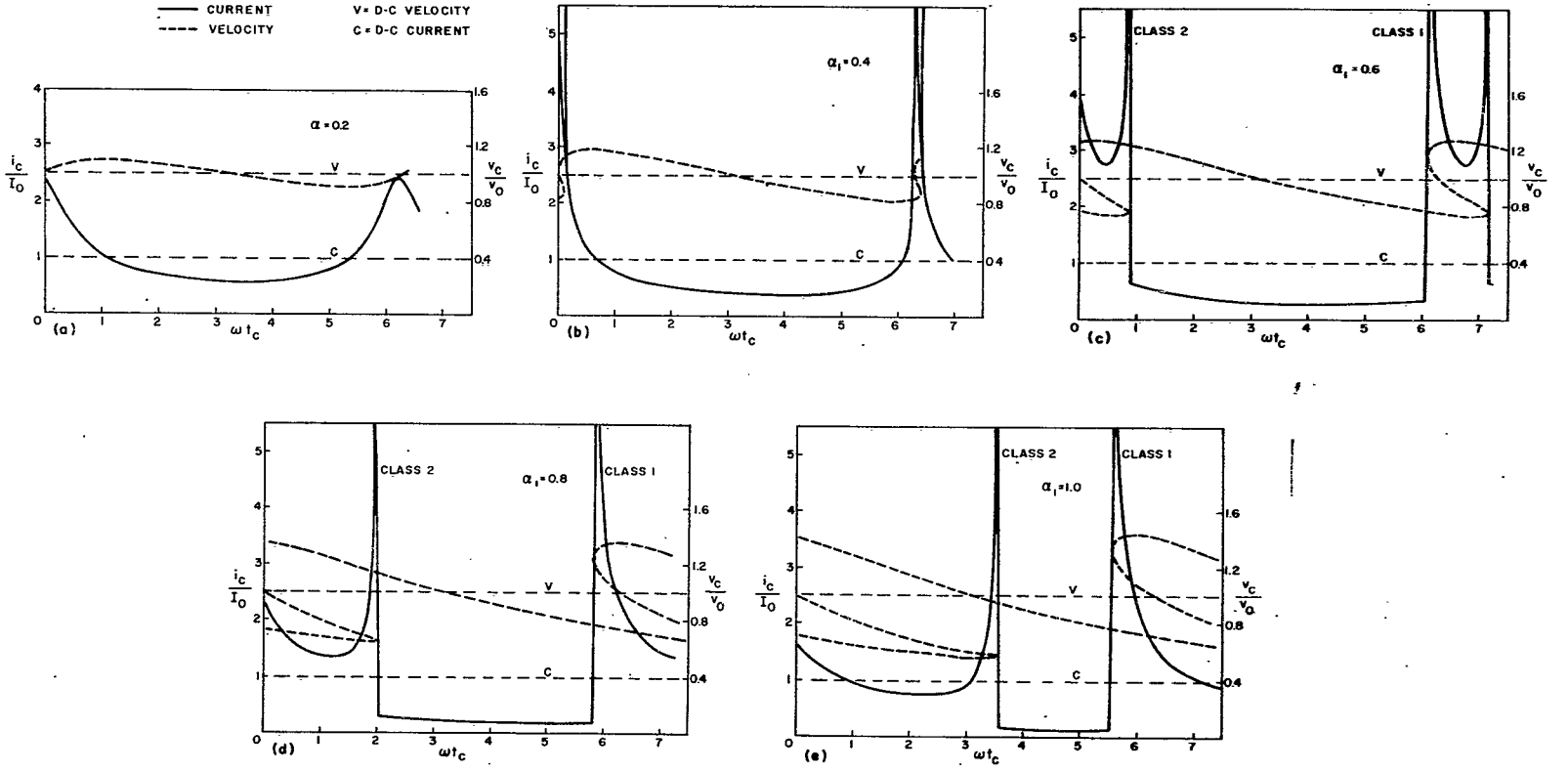

Figure 18. Normalized Entrance Current i_c/I_o versus Entrance Time ωt_c (solid line) and Normalized Entrance Velocity v_c/v_o versus Entrance Time ωt_c (broken line) for Different Depths of Modulation and $\theta_{g_1} = 1.75$ radians, $\theta_o = 2\pi$ radians.

the entrance to the second gap gan be divided into the following classes:

Class 1 - bunched fast electrons (near the first stationary point),
Class 2 - bunched slow electrons (near the first stationary point),
Class 3 - electrons near the second stationary point.

It is obvious from Figure 18 that as the depth of modulation a_1 is increased, two bunches of electrons occur, one of fast electrons (Class 1) and the other of slow electrons (Class 2). Since the drift angle θ_o is constant, Class 1 and Class 2 electrons begin to debunch at about $a_1 = 0.8$. The optimum bunching occurs between $a_1 = 0.6$ and $a_1 = 0.8$, which can also be easily predicted from Figure 17. The deviation of velocity from the d-c value increases as the depth of modulation a_1 is increased.

The operating parameters of this analysis are the depths of modulation at the first gap a_1, and at the second gap a_2, the d-c transit angle of the second gap θ_{g_2}, and the phase angle Γ_2 of the voltage V_2 across the second gap with respect to the fundamental component of the beam current at the entrance to the second gap. In the following analysis, therefore, one of these parameters will be varied while the other three parameters are held constant. Numerical calculations of Equation (4.17) using the computer data show the types of operation shown in Table I.

TABLE I.

Types of Operation Indicated by Computer Data

Type	Kinetic energy w (normalized)	Maximum value of exit velocity v_d/v_o (normalized)
Type 1	decrease	decrease
Type 2	decrease	increase
Type 3	increase	increase

Cases of Type 3 are automatically excluded, since they are not included in the present study, but they might be used to represent the middle cavity in an analysis of a three-cavity klystron. The amount of the decrease in the normalized kinetic energy is, in general, greater in Type 1 than in Type 2. Further computations for Type 1 show that the greatest decrease in maximum velocity does not necessarily accompany the maximum output power, and the operating parameters are different for each of these cases.

In Figures 19 – 28 and in Figure 31, each class of electrons will be designated so that the reader can refer to Figure 18 to get a clear picture of the behavior of the electron beam. Figure 19 shows, for $\alpha_1 = 0.8$, $\alpha_2 = 1.0$, and $\theta_{g_2} = \pi$, the normalized exit current i_d/I_o, and the normalized exit velocity v_d/v_o, as functions of the exit time ωt_d when Γ_2 is varied from 0 to $-\pi$ radians in $\pi/4$-radian steps. Since the gap width and the voltage across the gap are constant, this series of graphs corresponds to the cases where the magnitude of the r-f field is held constant and the phase of it with respect to the beam is shifted. It is seen that under these operating conditions Class 1 and Class 2 electrons undergo changes while Class 3 electrons (of which there are only a few) are affected very little. As Γ_2 is increased in the negative direction, the two bunches already existing come closer and form a single bunch. This bunching seems to be related to the velocity in such a manner that the maximum velocity of Class 1 electrons increases as the negativeness of Γ_2 is increased and as power is fed into the gap. The case for $\Gamma_2 = -\pi/4$ is the optimum operation for this series for output power, but the efficiency is very small since the bunch of Class 2 electrons is accelerated while the bunch of Class 1 electrons are decelerated in passing through the gap. Overtaking occurs within the

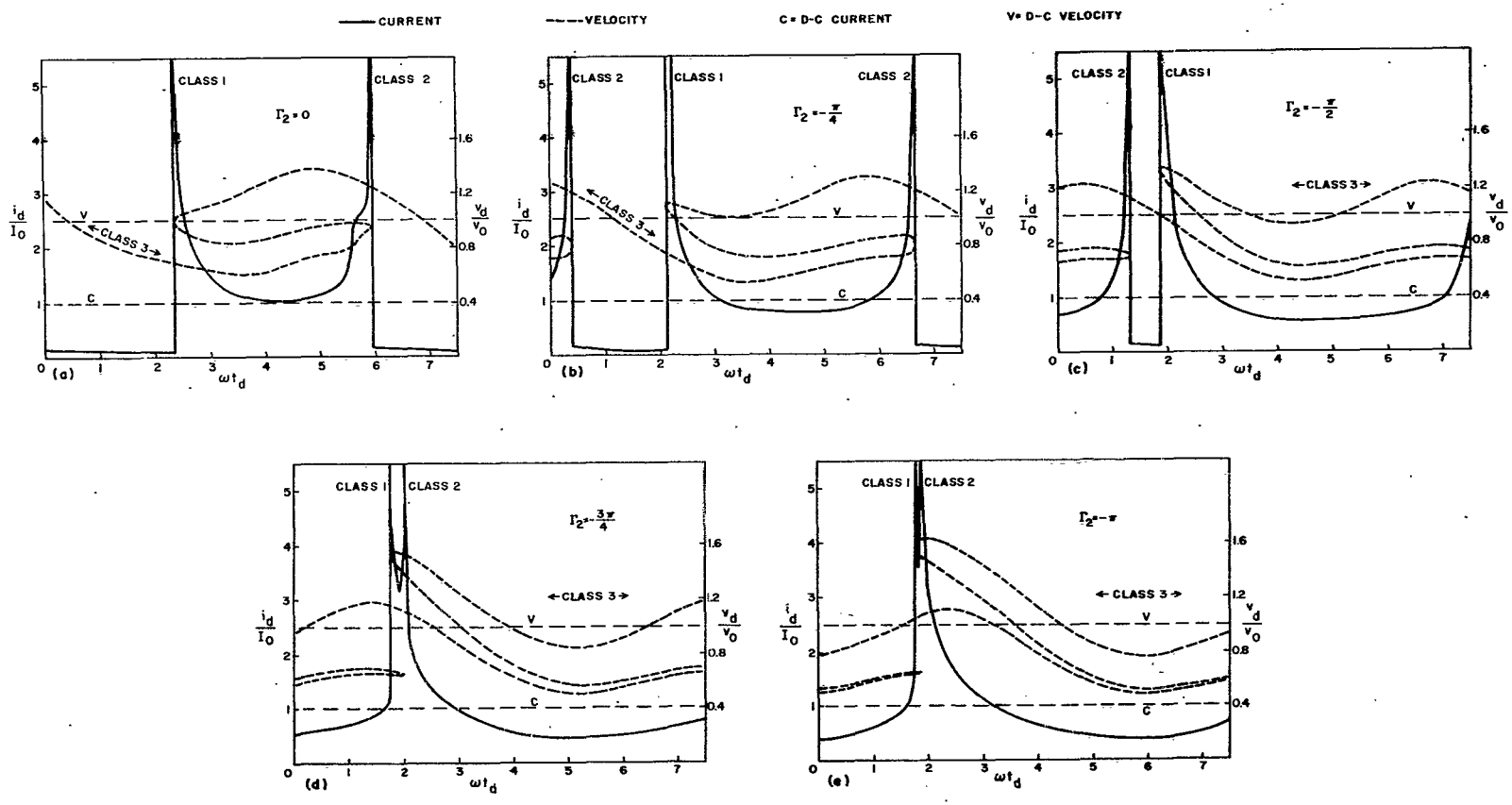

Figure 19. Normalized Exit Current i_d/I_o versus Exit Time ωt_d (solid line) and Normalized Exit Velocity v_d/v_o versus Exit Time ωt_d (broken line) for Different Phase Angles and $a_1 = 0.8$, $a_2 = 1.0$, and $\theta_{g_2} = \pi$.

gap between $\Gamma_2 = -\pi/2$ and $\Gamma_2 = -3\pi/2$.

Figure 20 shows, for $\alpha_1 = 0.8$, $\alpha_2 = 1.0$, and $\Gamma_2 = -\pi/2$, the normalized exit current, i_d/I_o, and the normalized exit velocity, v_d/v_o, as functions of the exit time ωt_d, when θ_{g_2} is varied from $3\pi/4$ to $7\pi/4$ radians in $\pi/4$-radian steps. As θ_{g_2} is increased, Class 1 and Class 2 electrons first bunch together, overtaking occurs within the gap, and then these two classes of electrons begin to debunch. It should be noticed that the magnitude of the r-f field decreases continuously in this series of graphs. The phase angle Γ_2 is such that both the bunch of Class 1 electrons and the bunch of Class 2 electrons are decelerated continuously from one case to the other. At the beginning of the series, power is fed into the gap for $\theta_{g_2} = 3\pi/4$ and $\theta_{g_2} = \pi$ cases, but it is taken out for the remaining cases. The case for $\theta_{g_2} = 7\pi/4$ represents the velocity-filter gap, in which there is a 10.3 per cent decrease in the maximum velocity, and the efficiency is 13.5 per cent.

Figure 21 shows, for $\alpha_1 = 0.8$, $\theta_{g_2} = \pi/2$, and $\Gamma_2 = -\pi/4$, the normalized exit current, i_d/I_o, and the normalized exit velocity, v_d/v_o, as functions of the exit time, ωt_d, when α_2 is varied from 0.2 to 1.0 in 0.2 steps. This series of graphs represents the catcher gap of a two-cavity klystron. In these cases, the debunching of the beam during one cycle and the phase angle Γ_2 are optimum for energy extraction from the beam. Velocity spread and efficiency increase as α_2 (and therefore the magnitude of the r-f field) is increased. Velocities of Class 1 electrons change little, but the amount of charge of this class of electrons decreases continuously. Velocities and the amount of charge of Class 2 electrons change drastically, and a split occurs in the bunch of Class 2 electrons.

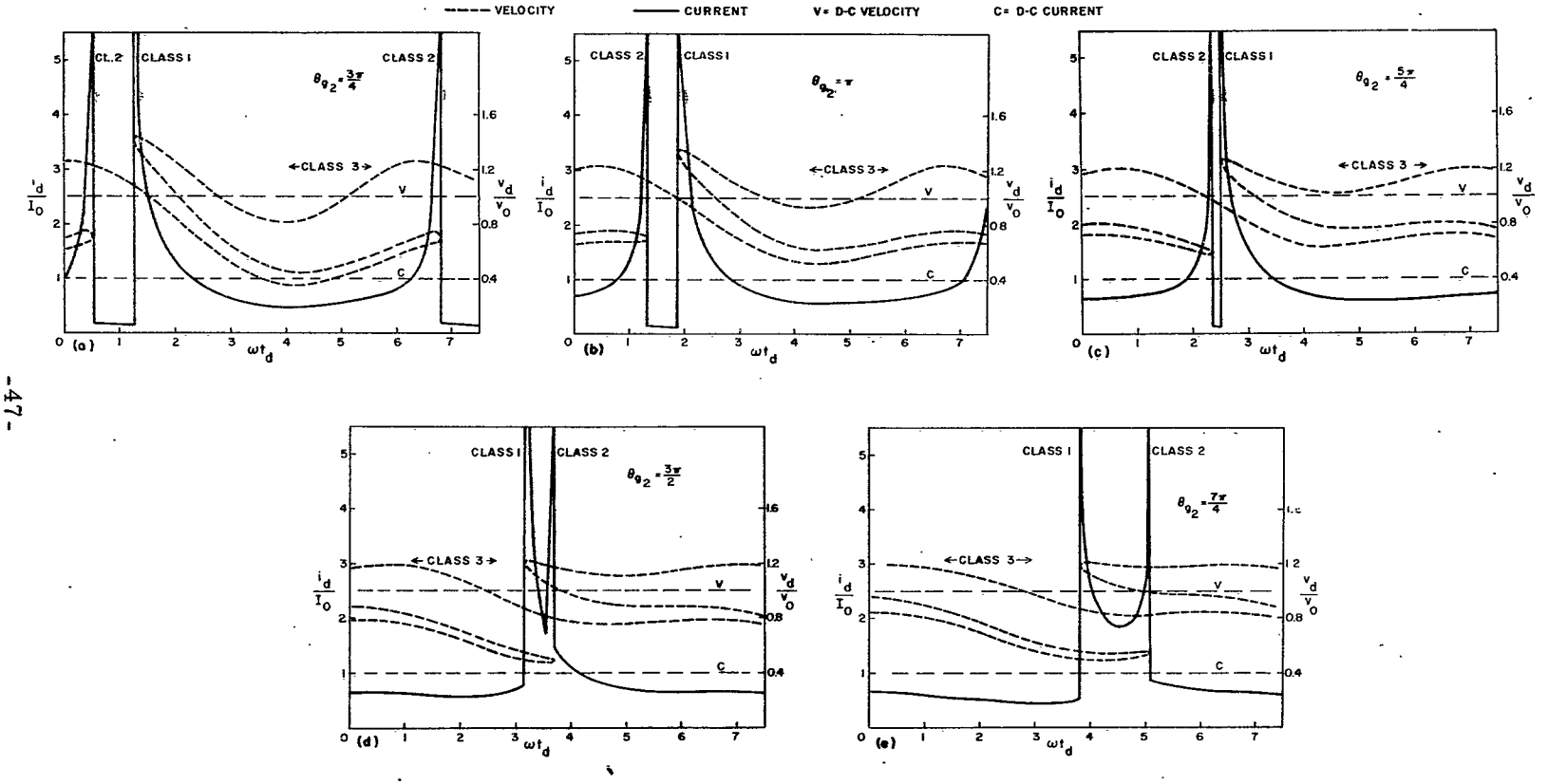

Figure 20. Normalized Exit Current i_d/I_o versus Exit Time ωt_d (solid line) and Normalized Exit Velocity v_d/v_o versus Exit Time ωt_d (broken line) for Different Gap Lengths and $a_1 = 0.8$, $a_2 = 1.0$, and $\Gamma_2 = -\pi/2$.

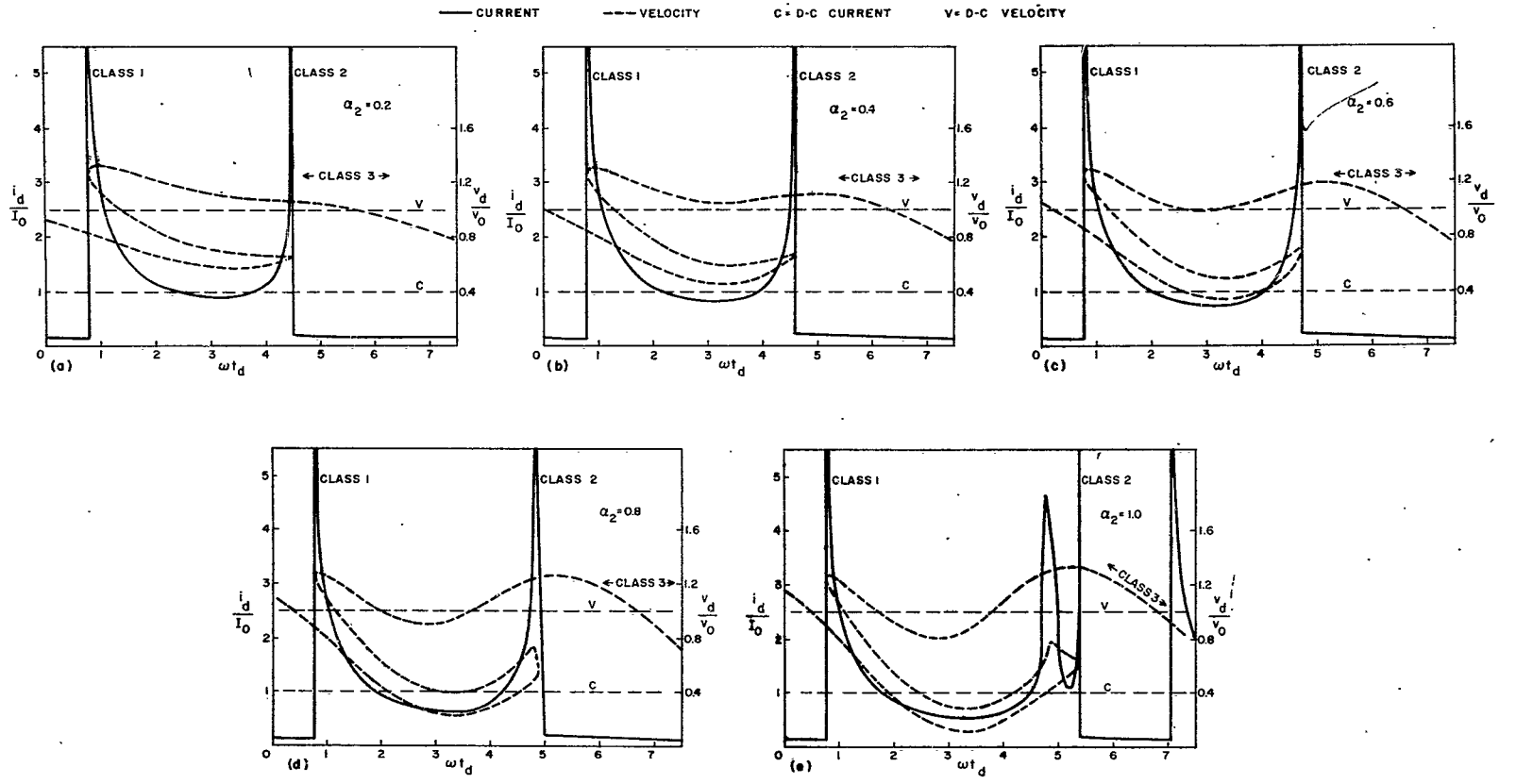

Figure 21. Normalized Exit Current i_d/I_o versus Exit Time ωt_d (solid line) and Normalized Exit Velocity v_d/v_o versus Exit Time ωt_d (broken line) for Different Depths of Modulation and $\alpha_1 = 0.8$, $\theta_{g_2} = \pi/2$, and $\Gamma_2 = -\pi/4$.

Class 3 electrons, on the other hand, fall out of phase and take energy from the r-f field; consequently their velocities (and hence their kinetic energies) increase.

Figure 22 shows, for $\alpha_1 = 0.8$, $\theta_{g_2} = 7\pi/4$, and $\Gamma_2 = -\pi/2$, the normalized exit current, i_d/I_o, and the normalized exit velocity, v_d/v_o, as functions of the exit time ωt_d, when α_2 is varied from 0.2 to 1.0 in 0.2 steps. This series of graphs represents the velocity-filter gap when the electron beam at the entrance is assumed to be a spent beam. Since the gap is long, overtaking within the gap has already occurred between Class 1 electrons and Class 2 electrons. They appear as a single split bunch. The debunching between the two classes of electrons increases as α_2 increases (therefore the magnitude of the r-f field increases), whereas Class 3 electrons pass through the gap almost unaffected. The interesting feature of this series of graphs is that whereas Class 1 electrons are being decelerated and are giving their energies to the r-f field, Class 2 electrons are accelerated and take energy from the r-f field. Velocity spreads, output powers, and efficiencies are smaller than those of the cases shown in Figure 21, but the extent of the decrease in the maximum normalized velocity is greater.

The behavior of the electron beam when it passes through the catcher gap of a two-cavity klystron and through the velocity-filter gap is shown in Figures 21 and 22 respectively. A better understanding can be obtained if, in addition, one examines the changes in the incremental charge Δq and in the incremental kinetic energy ΔW of electrons in a specific range of velocities. For this purpose bar graphs representing percentages of Δq and ΔW for ranges of velocities spanning ten per cent of the d-c velo-

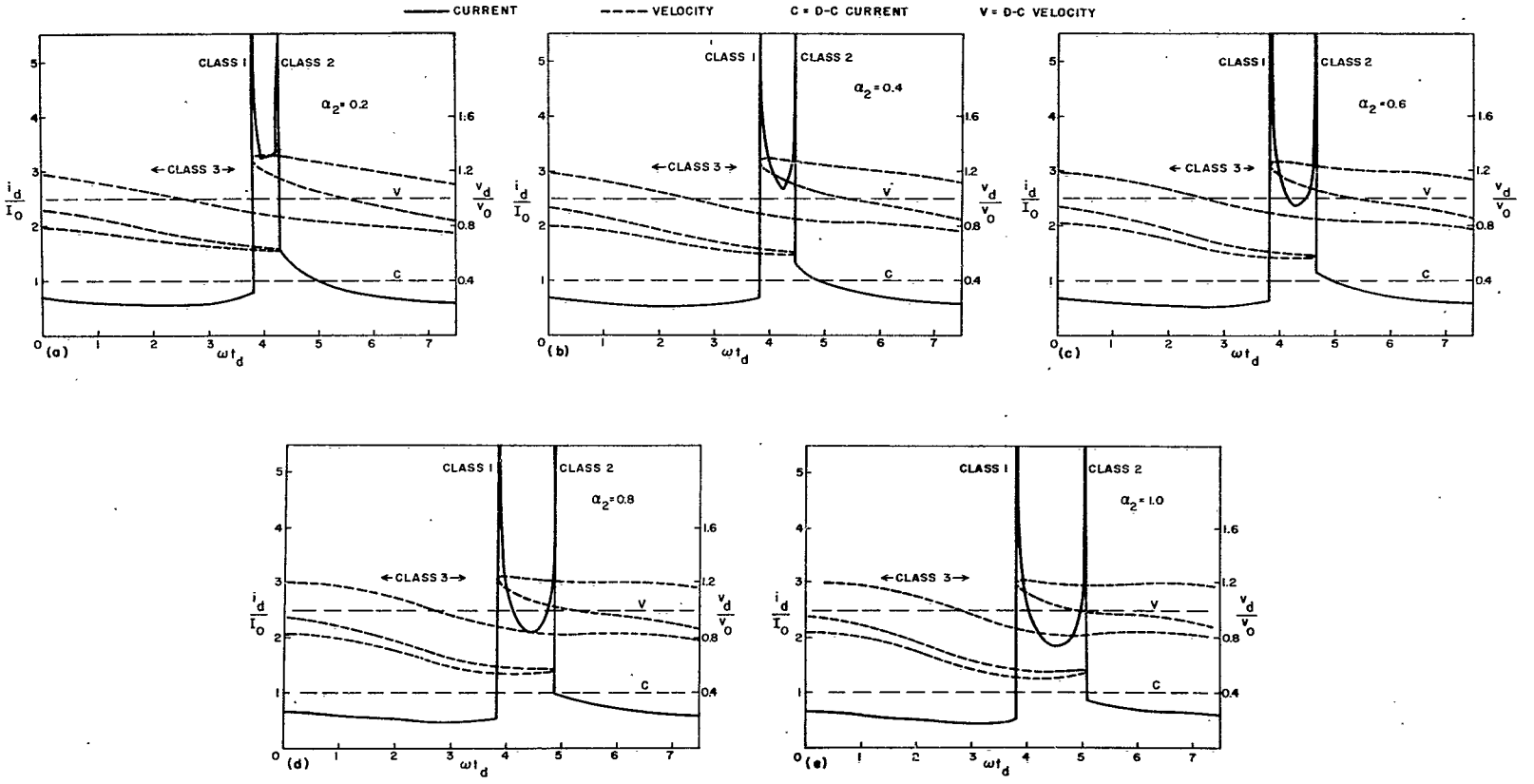

Figure 22. Normalized Exit Current i_d/I_o versus Exit Time ωt_d (solid line) and Normalized Exit Velocity v_d/v_o versus Exit Time ωt_d (broken line) for Different Depths of Modulation and $\alpha_1 = 0.8$, $\theta_{g_2} = 7\pi/4$, and $\Gamma_2 = -\pi/2$.

city are used. Each ten-per-cent span will be termed a velocity-class in this report. Electrons will be designated either by their velocity-class or as: (1) slow electrons – those having velocities less than the d-c velocity, (2) fast electrons – those having velocities more than the d-c velocity.

Figure 23 shows the percentage of incremental charge Δq, and the percentage of full incremental kinetic energy ΔW versus velocity-class at the entrance to the second gap for the case of $a_1 = 0.8$. It is seen that the total incremental charge is 49.264 per cent, the total incremental kinetic energy is 28.303 per cent for slow electrons; and the total incremental charge is 50.736 per cent, the total incremental kinetic energy is 71.697 per cent for fast electrons. It is also apparent that the charge is accumulated mostly at the extremes, and that this accumulation of charge corresponds to the existence of bunches in the beam at the entrance to the second gap. On the other hand, since the kinetic energy is proportional to the square of the velocity, the total kinetic energy of the fast electrons is about 2.5 times the total kinetic energy of the slow electrons, whereas the ratio of total charges is almost equal to one.

Figure 24 shows, for $a_1 = 0.8$, the percentage of incremental charge Δq versus the normalized velocity-class v_d/v_o, with a_2 as a parameter, at the exit of the catcher-gap selected (i.e., $\theta_{g_2} = \pi/2$ and $\Gamma_2 = -\pi/4$). In each case of this series of graphs except in Figure 24b, it is seen that the total percentage of Δq is decreased for fast electrons, and that the velocity spread is wider than that at the entrance, although the maximum velocity-class does not exceed 1.4. This obviously means that, on the average, the electrons are decelerated and power is taken out from the

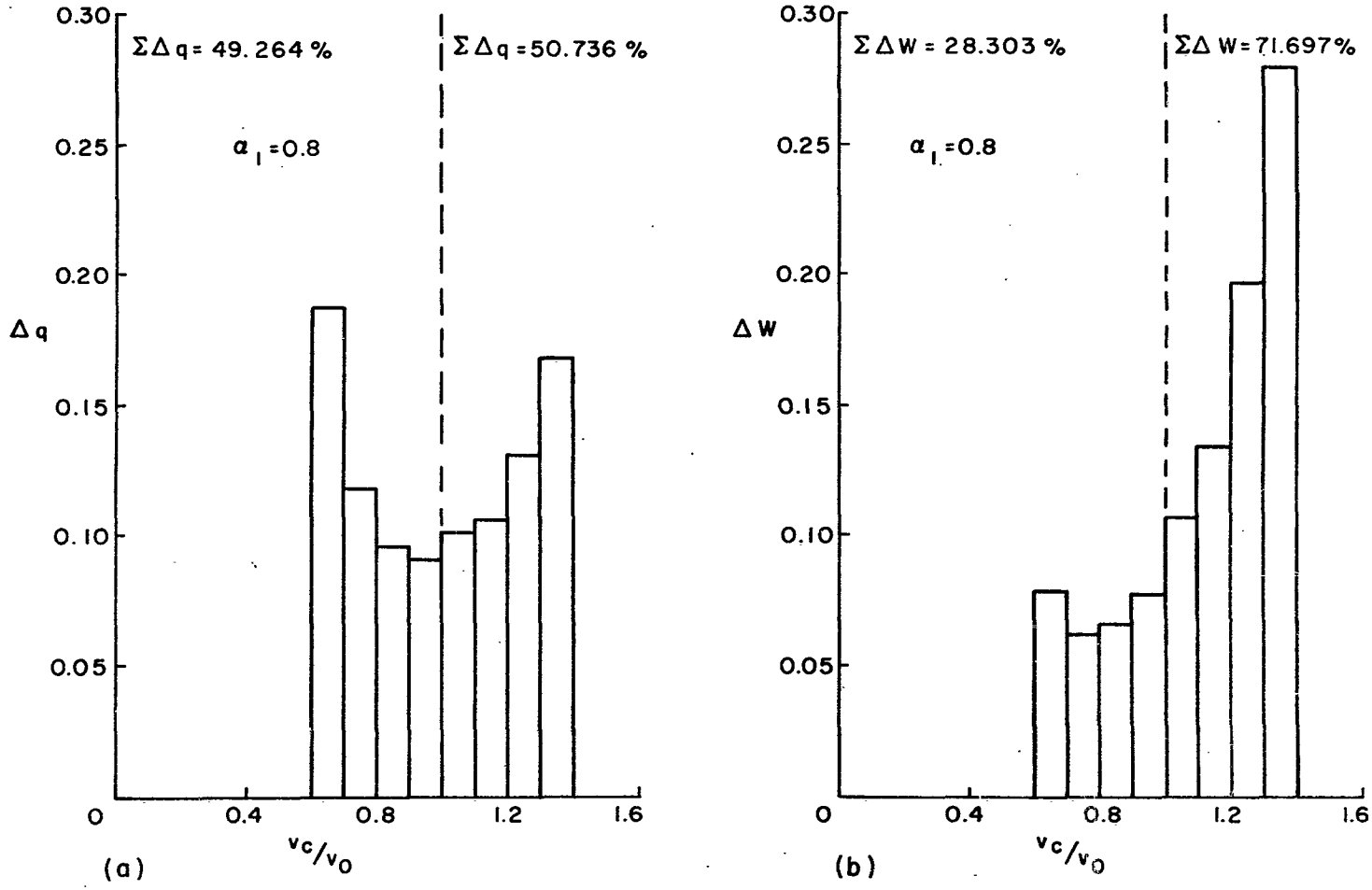

Figure 23. (a) Percentage of Incremental Charge Δq versus Velocity-Class v_d/v_o ; (b) Percentage of Incremental Kinetic Energy ΔW versus Velocity-Class v_d/v_o at Entrance to Second Gap for $\alpha_1 = 0.8$.

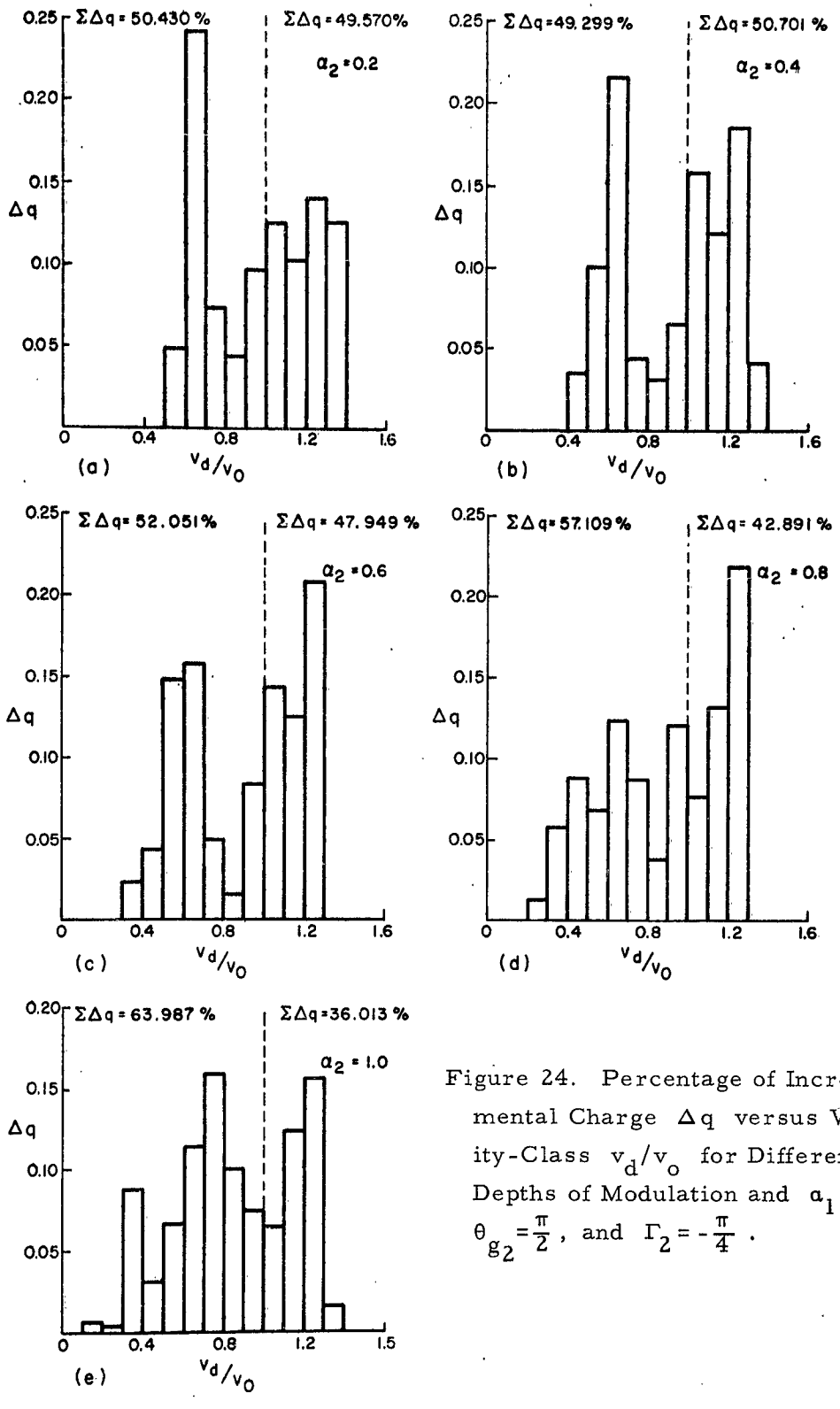

Figure 24. Percentage of Incremental Charge Δq versus Velocity-Class v_d/v_o for Different Depths of Modulation and $\alpha_1 = 0.8$, $\theta_{g_2} = \frac{\pi}{2}$, and $\Gamma_2 = -\frac{\pi}{4}$.

electron beam. The main effect of increasing the r-f field (i.e., increasing a_2) in this gap is to decelerate the electrons. In some velocity-classes, there is an increase in the percentage of Δq when a_2 is increased. This increase occurs because at the entrance to the gap, the electrons in a velocity-class have different phases with respect to the r-f voltage across the gap. Some of these electrons are accelerated while others are decelerated. To visualize this phenomenon, one should examine the adjacent velocity-classes. In Figure 24(d), for example, both the percentages of Δq for the velocity classes 1.1 and 1.2 show slight increases from the previous case. Examining the velocity-class 1.0 (i.e., 1.0 – 1.1), one can see that the decrease in this class of electrons is greater than the increase in the higher velocity-classes. In other words, a few of the electrons of velocity-class 1.0 are accelerated while a greater number of them are decelerated.

Bar graphs representing the percentage of incremental kinetic energy ΔW versus the normalized velocity-class, v_d/v_o, with a_2 as a parameter, are depicted in Figure 25 for the catcher gap selected. It is seen that as a_2 is increased, the total kinetic energy for the electron beam, as well as for the fast electrons, decreases continuously. The total kinetic energy for the slow electrons first decreases and then increases as a_2 is increased. This increase is not due to the acceleration of slow electrons, but is due mainly to the increase in their total charge. The changes in the total kinetic energy of the slow electrons are, however, only a few per cent. Observing the same phenomenon as in Figure 24(d), one can see that the percentages of ΔW for the two velocity-classes 1.1 and 1.2 show slight increases, but the decrease in the percentage of ΔW for the velocity-class 1.0 is greater

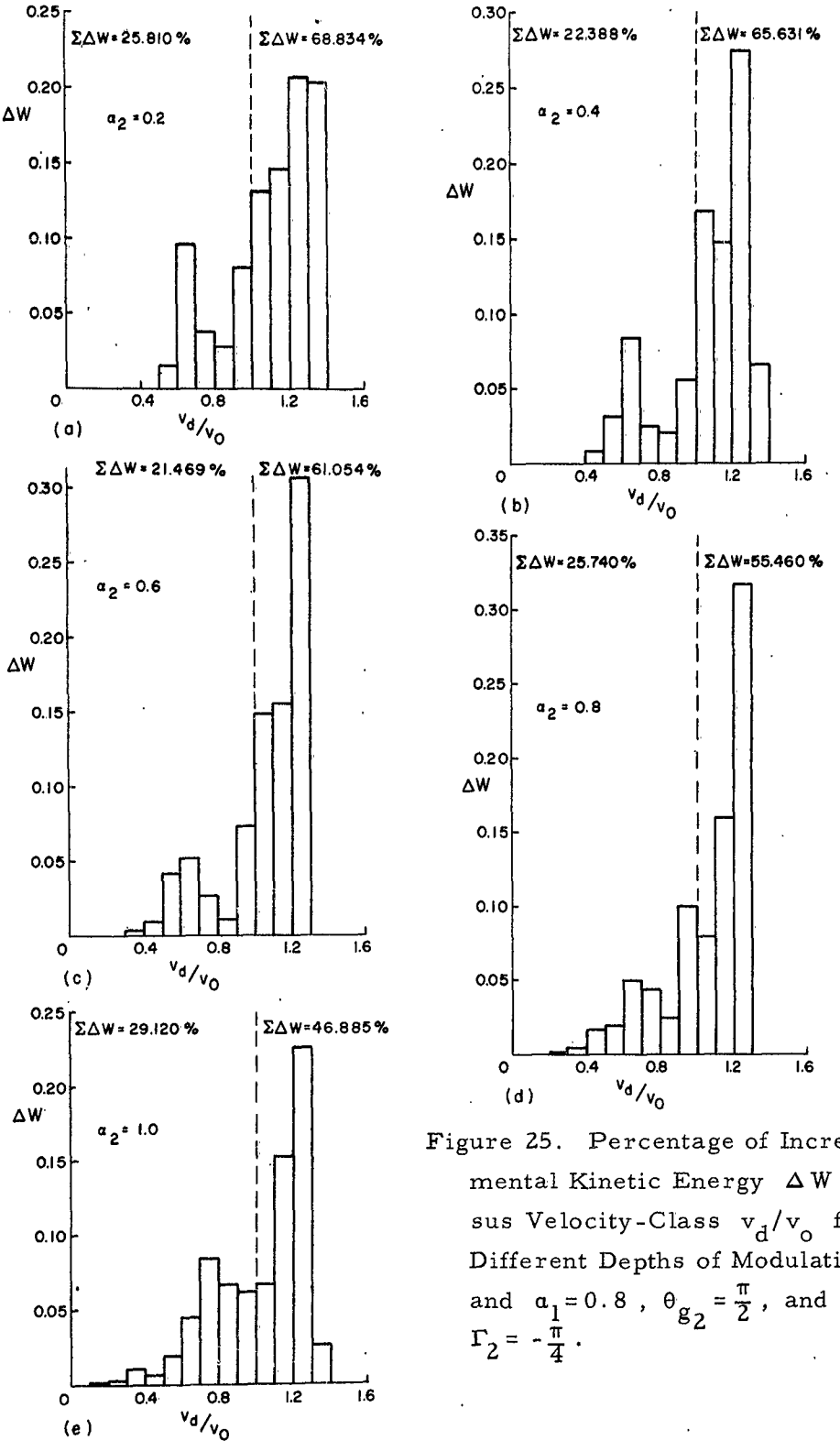

Figure 25. Percentage of Incremental Kinetic Energy ΔW versus Velocity-Class v_d/v_o for Different Depths of Modulation and $\alpha_1 = 0.8$, $\theta_{g_2} = \frac{\pi}{2}$, and $\Gamma_2 = -\frac{\pi}{4}$.

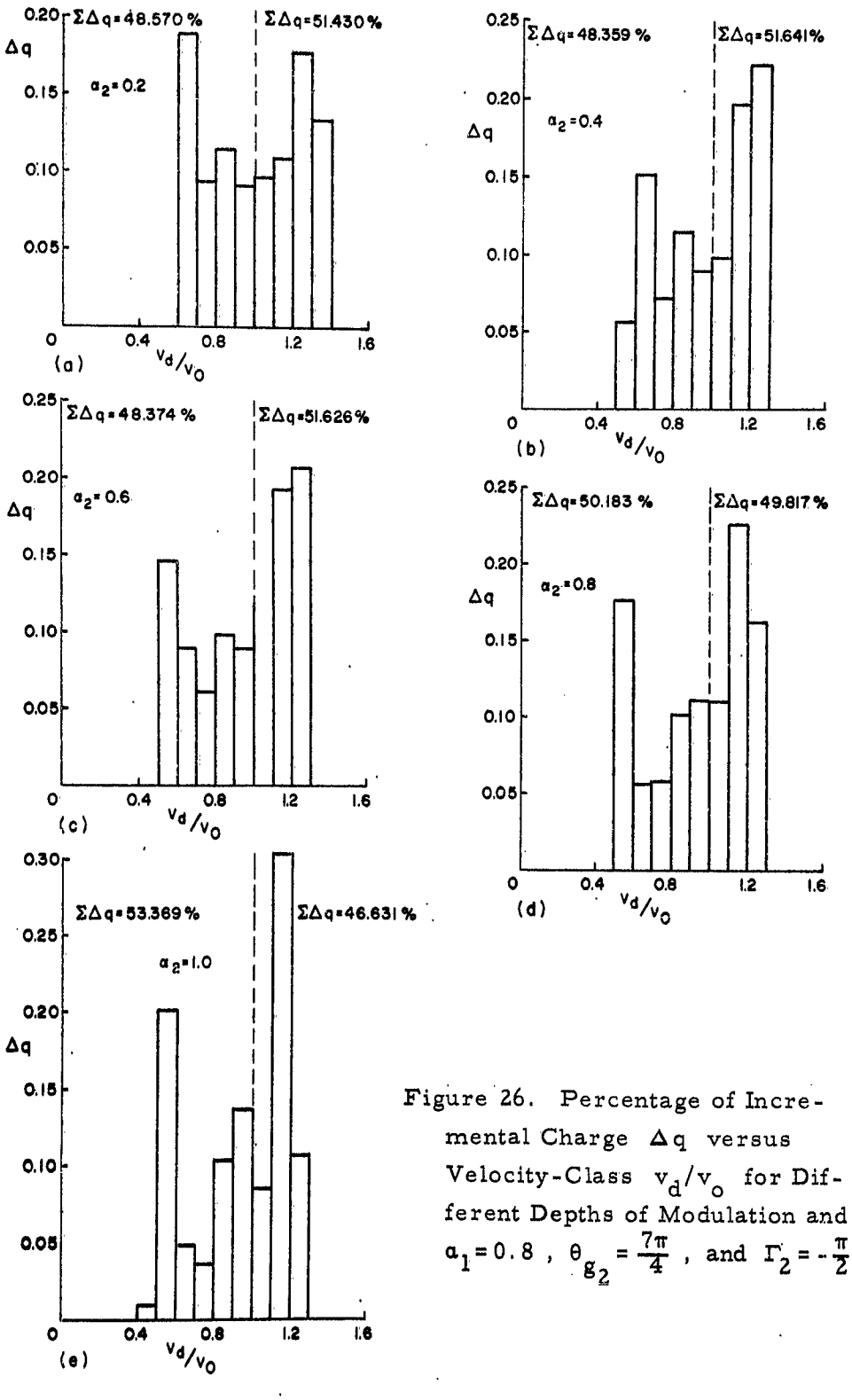

Figure 26. Percentage of Incremental Charge Δq versus Velocity-Class v_d/v_o for Different Depths of Modulation and $\alpha_1 = 0.8$, $\theta_{g_2} = \frac{7\pi}{4}$, and $\Gamma_2 = -\frac{\pi}{2}$.

than the increase in the higher velocity-classes.

Figure 26, which is similar to Figure 24, is for the velocity-filter gap selected (i.e., $\theta_{g_2} = 7\pi/4$, $\Gamma_2 = -\pi/2$), and for $\alpha_1 = 0.8$. The total percentages of Δq for both the slow electrons and the fast electrons change a few per cent as α_2 increases. The percentages of Δq of the velocity-classes higher than 1.2, however, decrease appreciably, from 30 per cent to 7.80 per cent. In contrast to this, the percentages of Δq of the velocity-classes lower than 0.7 increase from 18.75 per cent to 25.80 per cent.

Figure 27 shows the percentage of incremental kinetic energy ΔW versus the normalized velocity-class v_d/v_o, with α_2 as a parameter, for the selected velocity-filter gap. The total percentages of ΔW both for the electron beam and for the fast electrons decrease continuously, as expected from Figure 26, but as α_2 is increased the total percentages for the slow electrons first decrease and then increase. This increase is comparable to the increase in the total percentage of Δq, since most of the change occurs near the velocity-class 1.0.

An illustrative comparison between the catcher gap and the velocity-filter gap is shown in Figure 28. One salient point is the occurrence of over-taking within the gap in the case of the velocity-filter gap. The beam is also bunched more in the velocity-filter gap than in the catcher gap. On the other hand, the velocity spread of the electrons and hence the output power is larger in the catcher gap.

A numerical comparison between the catcher gap and the velocity-filter gap, selected as indicated, is given in Table II. In the table there are two columns for each case; the left column represents the percentage of decrease in maximum velocity, and the right column the percentage of power

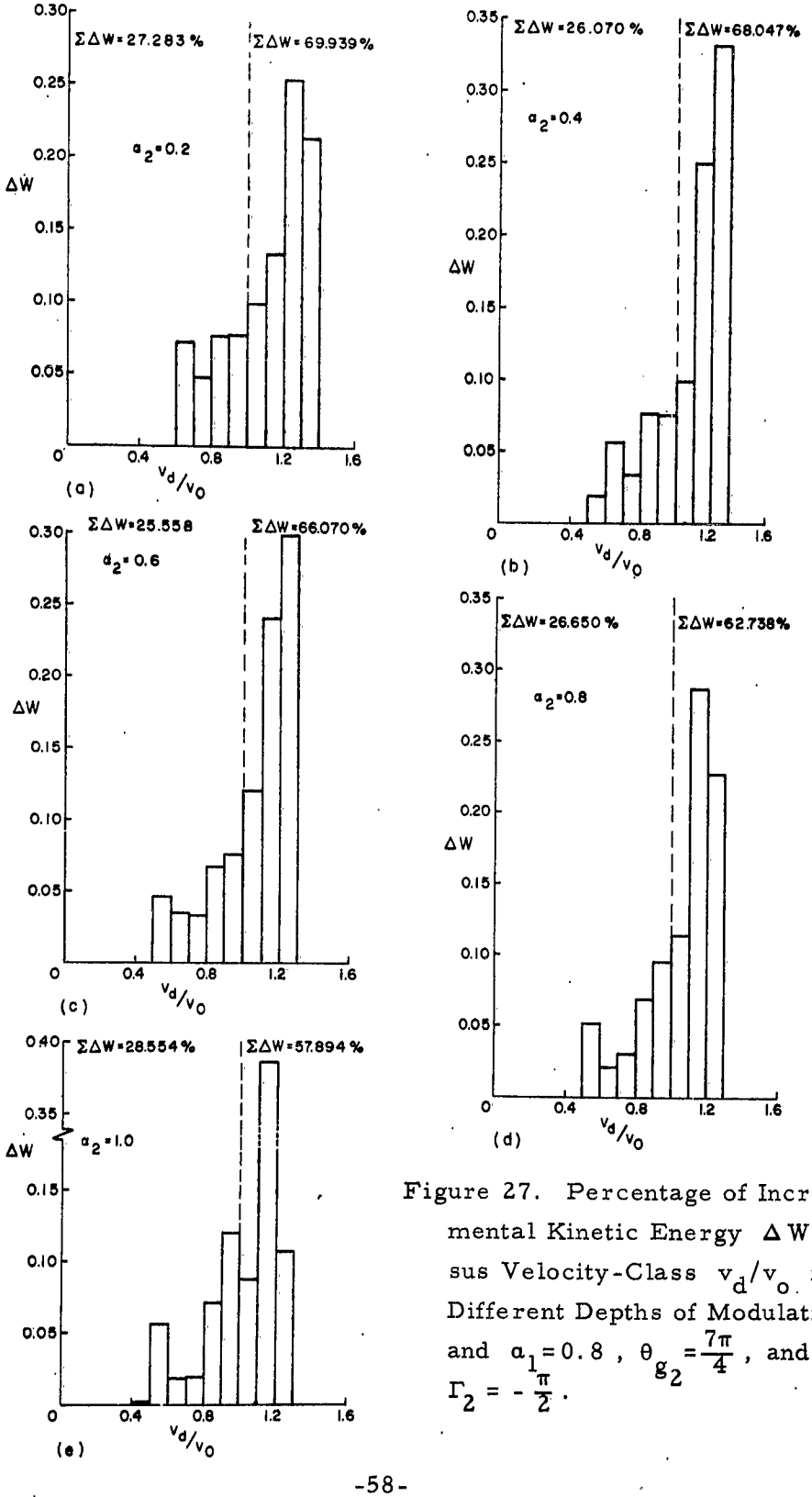

Figure 27. Percentage of Incremental Kinetic Energy ΔW versus Velocity-Class v_d/v_o for Different Depths of Modulation and $\alpha_1 = 0.8$, $\theta_{g_2} = \frac{7\pi}{4}$, and $\Gamma_2 = -\frac{\pi}{2}$.

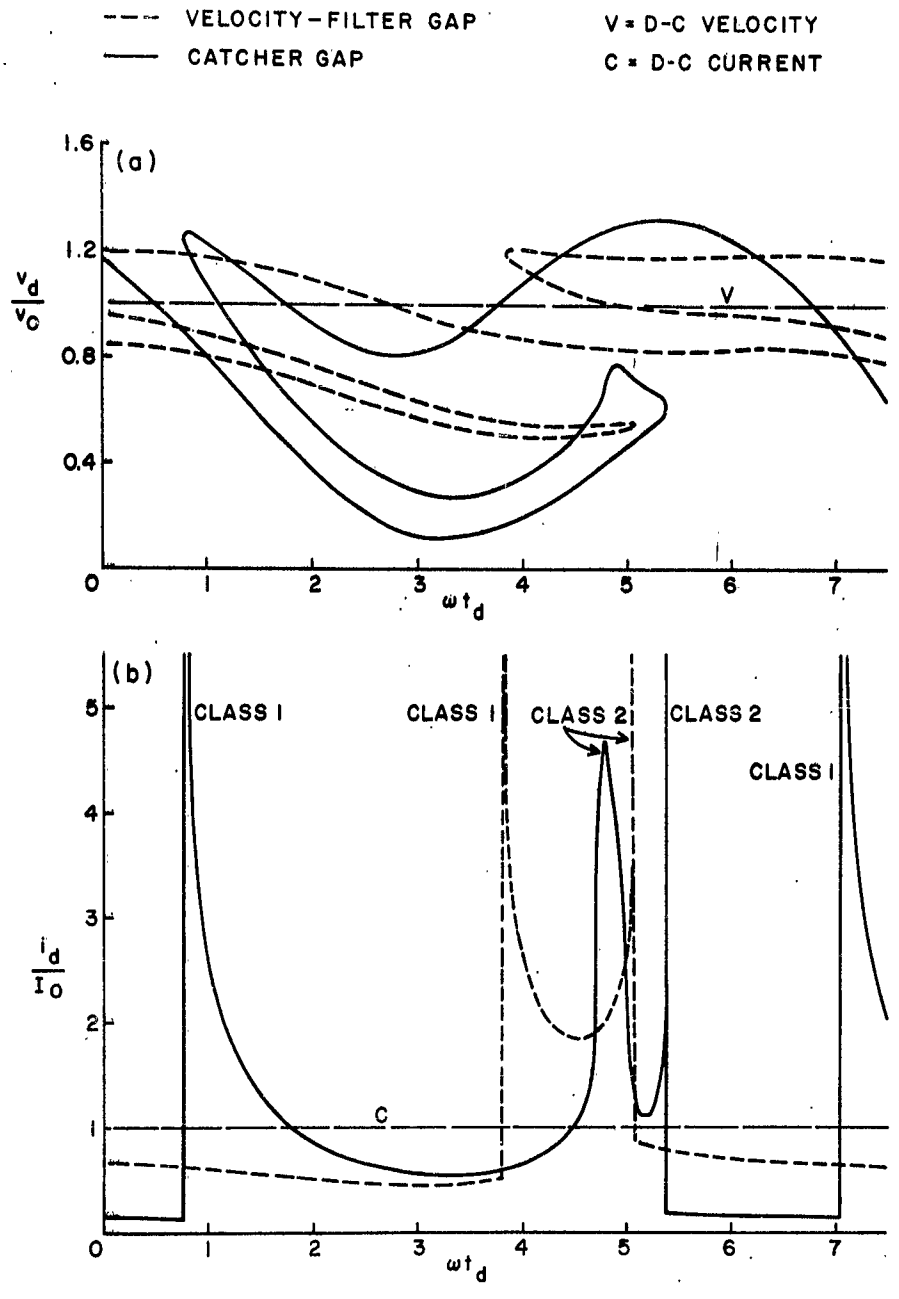

Figure 28. (a) Normalized Exit Velocity v_d/v_o versus Exit Time ωt_d; (b) Normalized Exit Current i_d/I_o versus Exit Time ωt_d for the Selected Catcher Gap (solid line) and for the Selected Velocity-Filter Gap (broken line).

TABLE II.

Velocity Decreases and Efficiencies
for Catcher Gap and for Velocity-Filter Gap

	$\theta_{g_2} = \pi/2$ $\Gamma_2 = -\pi/4$		$\theta_{g_2} = 7\pi/4$ $\Gamma_2 = -\pi/2$	
a_2	Velocity decrease (%)	Efficiency (%)	Velocity decrease (%)	Efficiency (%)
0.2	1.881	5.356	2.128	2.778
0.4	3.278	11.981	4.255	5.883
0.6	4.363	17.477	6.294	8.372
0.8	5.247	18.571	8.310	10.612
1.0	2.370	23.995	10.327	13.552

exchange. It is apparent that the decrease in maximum velocity is not proportional to output power in the case of the catcher gap, as it appears to be in the velocity-filter gap.

It can be concluded from the analysis of this chapter that at large signal levels one cannot easily predict the operating parameters for a catcher gap without calculating the kinetic energies at the entrance of the gap and at the exit from it. In contrast to this, the operating parameters for a velocity-filter gap can easily be predicted by the decrease in the maximum velocity at the exit from the gap. Efficiency of a velocity-filter gap is usually lower than that of a catcher gap, since slow electrons, being out of phase, are accelerated and take energy from the r-f field. This suggests elimination of slow electrons in a spent beam by some means, pre-

ferably electrostatic, before the beam is allowed to pass through a velocity-filter gap.

2. Loading Conditions of a Two-Cavity Klystron

It was previously mentioned that the existence of the assumed voltage V_2 across the second gap depends upon the physical realizability of the circuit parameters. Once the operating parameters and the power exchange for the second gap are known from the preceding analysis, the circuit parameters can be determined.

The equivalent circuit for the second gap is shown in Figure 29, where G_T represents the total conductance, and B_T represents the total susceptance of the cavity proper; i.e.,

$$G_T = G_l + G_c + G_b \quad , \tag{4.18}$$

$$B_T = B_l + B_c + B_b \quad , \tag{4.19}$$

where

G_l = load conductance referred to the cavity,

G_c = conductance representing the circuit loss in the cavity,

G_b = beam-loading conductance,

B_l = load susceptance referred to the cavity,

B_c = susceptance representing the tuning of the cavity,

B_b = beam-loading susceptance,

I_i = induced current at the cavity.

Figure 29b shows the vector diagram for the fundamental component of the entrance current i_{c_1} and the voltage V_2 across the second gap.

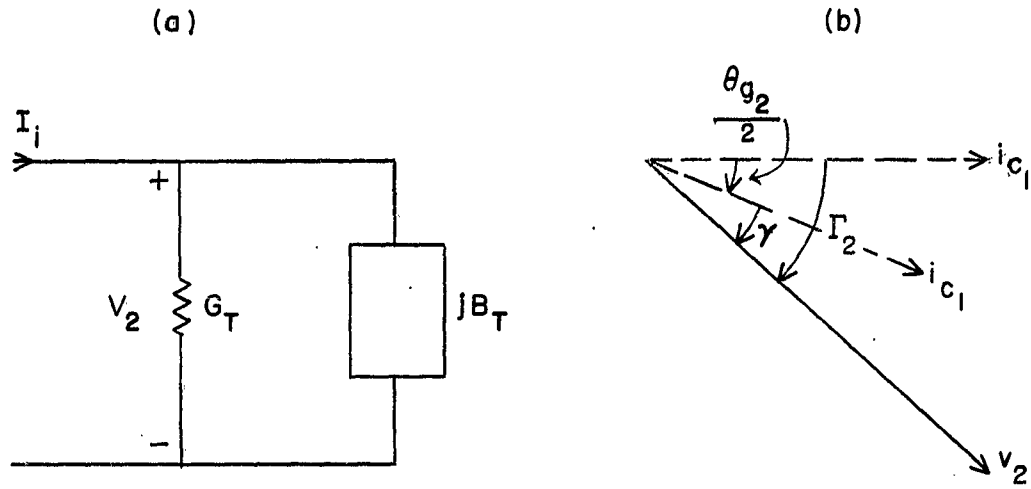

Figure 29. (a) Equivalent Admittance Circuit for Second Gap, (b) Vector Diagram for Fundamental Component of Entrance Current i_c, and Voltage V_2 across Second Gap.

When the reference is shifted to the center of the gap, the phase angle γ between i_{c_1} and V_2 represents the phase angle of the total admittance shown in Figure 29a if the cavity has a high Q; that is, if no harmonics are present in the induced current. The difference between the calculated kinetic energies at the entrance and exit of the second gap represents the power transferred to the load and the power dissipated in the cavity. One can then write

$$P_k = \frac{W_{k_{entrance}} - W_{k_{exit}}}{2\pi} \quad , \tag{4.20}$$

$$P_k = \frac{G' V_2^2}{2} \quad , \tag{4.21}$$

where

$$G' = G_l + G_c \quad . \tag{4.22}$$

One can thus determine the load conductance G_l referred to the cavity from Equations (4.20) – (4.22) and from measured values of Q_o and Q_x of the cavity.

V. ANALYSIS OF SECOND DRIFT SPACE AND LAST CAVITY

In this chapter it is assumed that the operating characteristics of the catcher gap and the velocity filter gap are as determined in the previous chapter, Because of the complexity of obtaining analytical formulas for the current and the velocity of the beam as functions of exit time, ωt_d, at the exit from the second gap, only computer solutions are sought for these characteristics. Also, in the formulation of the problem, which follows, the total current is not calculated; instead, current contributions from the increments of different ωt_c times are traced along the tube. Thus the physical phenomena taking place at any point along the tube are readily understood. The analysis here is similar to that of Chapter IV. The known characteristics of the catcher gap will provide the initial conditions at the entrance to the second drift space, and the known characteristics of the velocity-filter gap will be used as those of the third gap.

A. COMPUTER PROBLEM

Since the second drift space is again assumed to be a field-free space, the equation of motion is

$$\ddot{z} = 0 \quad . \tag{5.1}$$

The time at plane e (see Figure 30) can be expressed as

$$\omega t_e = \omega t_d + \frac{\theta_{o2}}{v_d/v_o} \quad , \tag{5.2a}$$

$$\theta_{o2} = \frac{\omega l_2}{v_o} \quad . \tag{5.2b}$$

Integrating Equation (5.1) once and applying the boundary conditions at $t = t_d$, one obtains

$$\frac{v_e}{v_o} = \frac{v_d}{v_o} \quad , \tag{5.3}$$

where v_d/v_o is given numerically by the computer. Differentiating Equation (5.2a) with respect to ωt_d, one obtains

$$\frac{d\omega t_e}{d\omega t_d} = 1 - \frac{\frac{\omega l_2}{v_o} \frac{d}{d\omega t_d}\left(\frac{v_d}{v_o}\right)}{\left(\frac{v_d}{v_o}\right)^2} \quad . \tag{5.4}$$

From Equation (4.8), one can derive

$$\frac{d}{d\omega t_d}\left(\frac{v_d}{v_o}\right) = \frac{\frac{d}{d\omega t_c}\left(\frac{v_c}{v_o}\right) + \frac{a_2}{2\theta_{g_2}} \sin(\omega t_c + \xi)}{\frac{d\omega t_d}{d\omega t_c}} - \frac{a_2}{2\theta_{g_2}} \sin(\omega t_d + \xi) \quad ; \tag{5.5}$$

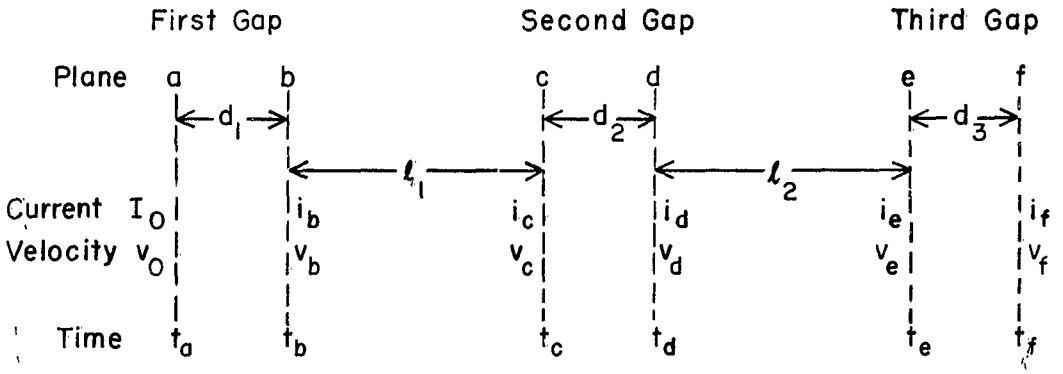

Figure 30. Schematic Diagram of the Combination of a Two-Cavity Klystron and a Velocity-Filter Gap.

$d\omega t_d/d\omega t_c$ is given in Equation (4.1) and $d(v_c/v_o)/d\omega t_c$ in Equation (4.16). Using the principle of conservation of charge for the second drift space, one obtains

$$\frac{i_e}{I_o} = \frac{\frac{i_d}{I_o}}{\left|\frac{d\omega t_e}{d\omega t_d}\right|} \quad . \tag{5.6}$$

Equations (5.2) – (5.6) define the normalized current, i_e/I_o, and the normalized velocity, v_e/v_o, as functions of time, ωt_e, corresponding to specific ωt_c times.

Assuming a voltage V_3 across the gap with a total phase Γ_3 with respect to the fundamental current at the entrance, one can write the equation of motion for the third gap as

$$\ddot{z} = -\frac{e}{m}\frac{V_3}{d}\sin(\omega t + \Gamma_3) \quad . \tag{5.7}$$

Integrating Equation (5.7) twice, substituting initial conditions at $t = t_e$, and normalizing with respect to d-c velocity, one obtains

$$\dot{Z} = \frac{v_e}{v_o} + \frac{a_3}{2\theta_{g_3}}\left[\cos(\omega t + \Gamma_3) - \cos(\omega t_e + \Gamma_3)\right] \quad , \tag{5.8}$$

and

$$Z = \left[\frac{v_e}{v_o} - \frac{a_3}{2\theta_{g_3}}\cos(\omega t_e + \Gamma_3)\right](t - t_e) + \frac{a_3}{2\omega\theta_{g_3}}\left[\sin(\omega t + \Gamma_3) - \sin(\omega t_e + \Gamma_3)\right] \quad , \tag{5.9}$$

where a_3 is the ratio of the assumed voltage, V_3, to the d-c beam voltage V_o, and the d-c gap transit angle, θ_{g_3}, is defined by

$$\theta_{g_3} \equiv \frac{\omega d_3}{v_o} \quad . \tag{5.10}$$

Applying boundary conditions at $t = t_f$ to Equations (5.8) and (5.9) and multiplying the latter by ω gives the following equations:

$$\theta_{g_3} = \left[\frac{v_e}{v_o} - \frac{a_3}{2\theta_{g_3}} \cos(\omega t_e + \Gamma_3)\right] (\omega t_f - \omega t_e)$$

$$+ \frac{a_3}{2\theta_{g_3}} \left[\sin(\omega t_f + \Gamma_3) - \sin(\omega t_e + \Gamma_3)\right] \quad , \tag{5.11}$$

$$\frac{v_f}{v_o} = \frac{v_e}{v_o} + \frac{a_3}{2\theta_{g_3}} \left[\cos(\omega t_f + \Gamma_3) - \cos(\omega t_e + \Gamma_3)\right] \quad . \tag{5.12}$$

Equation (5.11) is used to compute the exit time, ωt_f, and Equation (5.12) to compute the normalized exit velocity, v_f/v_o.

The principle of conservation of charge for the third gap results in

$$\frac{i_f}{I_o} = \frac{\frac{i_e}{I_o}}{\left|\frac{d\omega t_f}{d\omega t_e}\right|} \quad . \tag{5.13}$$

The denominator of Equation (5.13) is found by differentiating Equation (5.11) with respect to ωt_e; therefore

$$\frac{d\omega t_f}{d\omega t_e} = \frac{\frac{v_e}{v_o} - \frac{a_3}{2\theta_{g_3}} (\omega t_f - \omega t_e) \sin(\omega t_e + \Gamma_3) - (\omega t_f - \omega t_e) \frac{d}{d\omega t_e} \frac{v_e}{v_o}}{\frac{v_e}{v_o} + \frac{a_3}{2\theta_{g_3}} \left[\cos(\omega t_f + \Gamma_3) - \cos(\omega t_e + \Gamma_3)\right]} \quad , \tag{5.14}$$

where

$$\frac{d}{d\omega t_e}\left(\frac{v_e}{v_o}\right) = \frac{d\omega t_d}{d\omega t_e}\ \frac{d}{d\omega t_d}\left(\frac{v_d}{v_o}\right) = \frac{\dfrac{d}{d\omega t_d}\left(\dfrac{v_d}{v_o}\right)}{\dfrac{d\omega t_e}{d\omega t_d}} \quad . \qquad (5.15)$$

It should be noted that since all the derivatives are single-valued, the reversal of the derivatives at various stages of this analysis is valid. This is a result of considering the components only, rather than the total contributions of current from the increments of ωt_c time. Total currents and corresponding velocities can be plotted from computer data at any major point along the tube.

B. VELOCITY FILTERING

Equations (5.2) – (5.6) for the second drift space and Equations (5.11) – (5.15) for the third gap were computed by the digital computer. Since the operating parameters of the catcher gap and the velocity-filter gap were known, they were used as constants of the problem, with the normalized second drift angle θ_{o2} as a variable.

One can see from Figure 28a that Class 1 electrons and Class 3 electrons have almost the same velocity, and they are almost π radians apart. The drifting of the electron beam in the second drift space, therefore, will not alter their relative positions with respect to each other. Consequently, in the third gap, with the known operating parameters for the velocity-filter gap, Class 3 electrons will be accelerated while Class 1 electrons are decelerated. This will result in a greater maximum normalized velocity in the electron beam at the exit from the third gap than

that at the exit from the second gap, which can be shown to be an improvement so far as the intensities of the X-ray radiation are concerned, since the amount of charge of Class 1 electrons is very much larger than that of Class 3 electrons. These intensities are calculated and discussed in the latter part of this chapter.

The computer data have shown that for the velocity-filter gap to be most effective on Class 1 electrons, the optimum drift angle θ_{o2} must be $9\pi/4$. The normalized exit current, i_f/I_o, and the normalized exit velocity, v_f/v_o, as functions of the exit time, ωt_f, are shown for the optimum case in Figure 31 where $\theta_{o2} = 9\pi/4$, $\theta_{g3} = 7\pi/4$, $\Gamma_3 = -\pi/2$, and $\alpha_3 = 1.0$. Each number on the curve shown in Figure 31a is the number assigned to an electron at plane c (Figure 30), which is chosen as an initial condition for the computer problem of Chapter IV. (The initial conditions at plane c for $\alpha_1 = 0.8$ are given in Appendix I.) It is apparent from Figure 31a that several overtakings occur, some in the second drift space and some in the third gap. These are due mainly to the large velocity spread in the electron beam at the exit from the catcher gap. The important groups of electrons are the decelerated Class 1 electrons and the accelerated Class 3 electrons. The rest are used only to compute the total kinetic energy of the electron beam. Bar graphs similar to those previously used are shown in Figure 32. If Figure 32a is compared to Figure 24e, it is apparent that, following the velocity-filter gap, the two bunches existing in the electron beam shift to lower velocities, but a small percentage of electrons (of Class 3) shift to higher velocities. The velocity spread, therefore, is somewhat the same as it was at the exit from the second gap. Both these shifts can again be seen if Figure 32b is compared to Figure 25e. It should be noted that

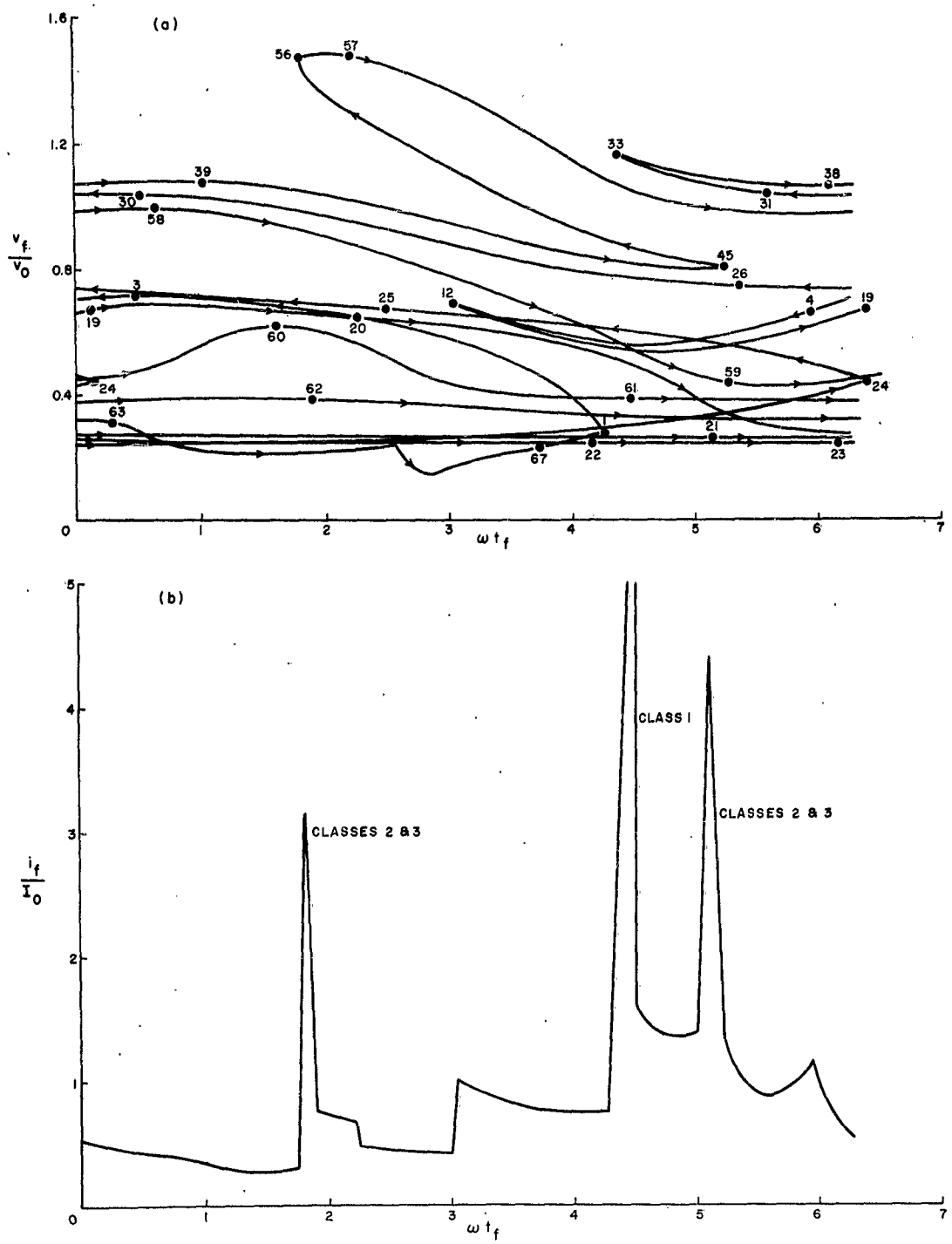

Figure 31. (a) Normalized Exit Velocity v_f/v_o versus Exit Time ωt_f; (b) Normalized Exit Current i_f/I_o versus Exit Time ωt_f for $L_2 = 9\pi/4$, $\theta_{g_3} = 7\pi/4$, $\Gamma_3 = -\pi/2$, and $\alpha_3 = 1.0$.

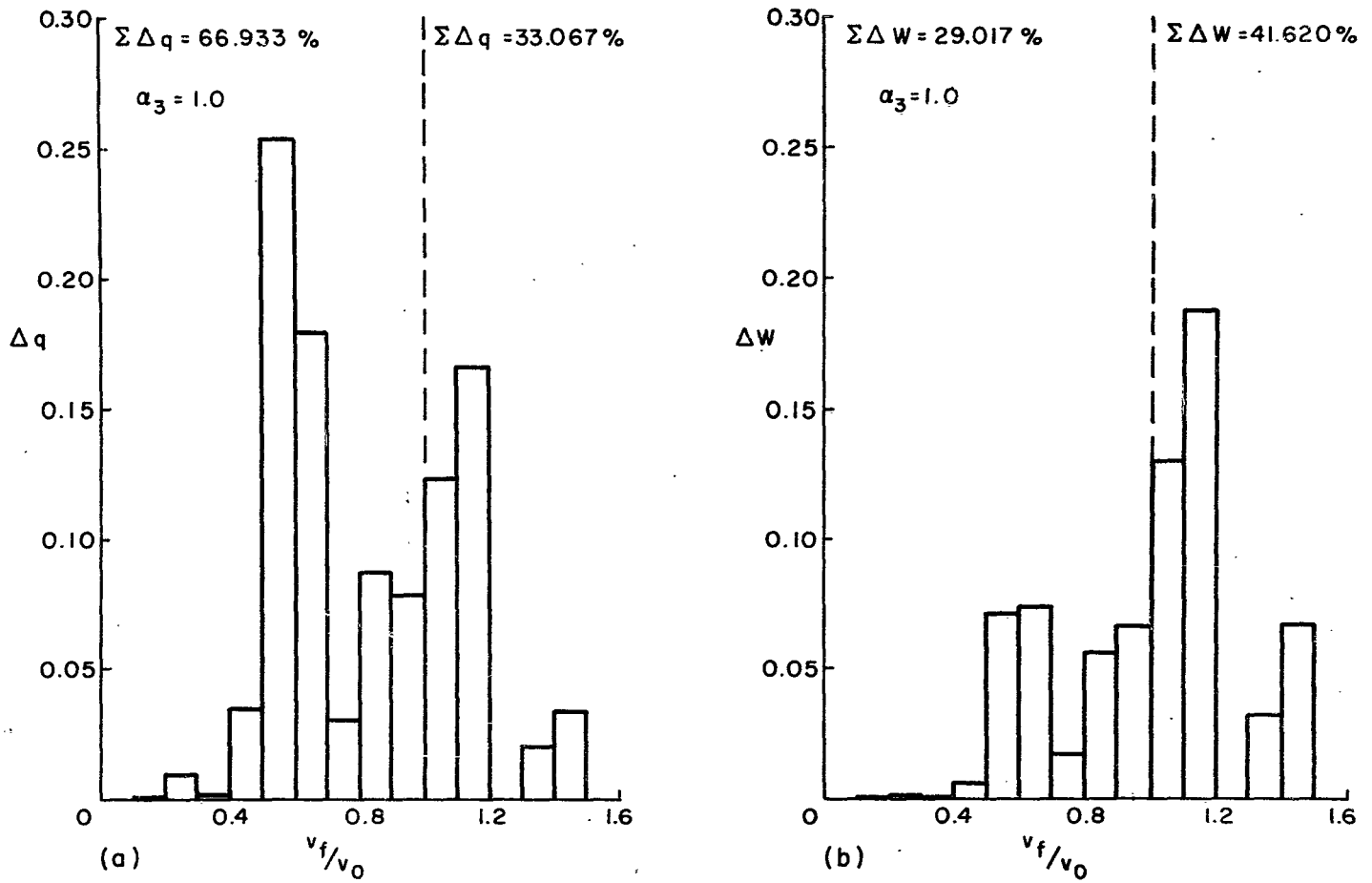

Figure 32. (a) Percentage of Incremental Charge Δq versus Velocity-Class v_f/v_o ; (b) Percentage of Incremental Kinetic Energy ΔW versus Velocity-Class v_f/v_o for $L_2 = \frac{9\pi}{4}$, $\theta_{g_3} = \frac{7\pi}{4}$, $\Gamma_3 = -\frac{\pi}{2}$, and $\alpha_3 = 1.0$.

for slow electrons the total incremental kinetic energy, $\Sigma\Delta W$, does not show an increase, but for fast electrons it shows a definite decrease. This is as expected, since the velocity-filter gap selected interacts primarily with the fast electrons. The calculations of the total kinetic energy show that the power is taken out and that the efficiency of the selected velocity-filter gap is 5.368 per cent.

The power taken out from the velocity-filter gap represents a further decrease in the total kinetic energy of the spent beam and hence a decrease in the total X-ray radiation from the collector (the target). Because of unavoidable phases and velocities of Class 3 electrons, the hardness of this radiation increases. In spite of this, the introduction of the velocity-filter gap produces an improvement in X-ray radiation simply by decelerating the highly bunched Class 1 electrons. In the following discussion the transmission of the continuous X-ray spectrum (Bremsstrahlung) through a given shield will be considered, and the transmitted intensities of variou wavelengths, with and without the velocity-filter gap, will be compared.

The continuous X-ray spectrum has some interesting features. The wavelength characteristics of the continuous spectrum are independent of the material of the target, but are determined by the voltage applied to the tube (see Figure 33). It is seen from Figure 33 that for a definite voltage, no radiation occurs up to a certain wavelength, (λ_{min}). "Having passed this wavelength, the intensity rises sharply to a maximum, and then gradually falls to a relatively low value. The intensity of the continuous spectrum is dependent on the target material, the tube current and the applied voltage as well as on the thickness of the target."[8,9] It was shown that the con-

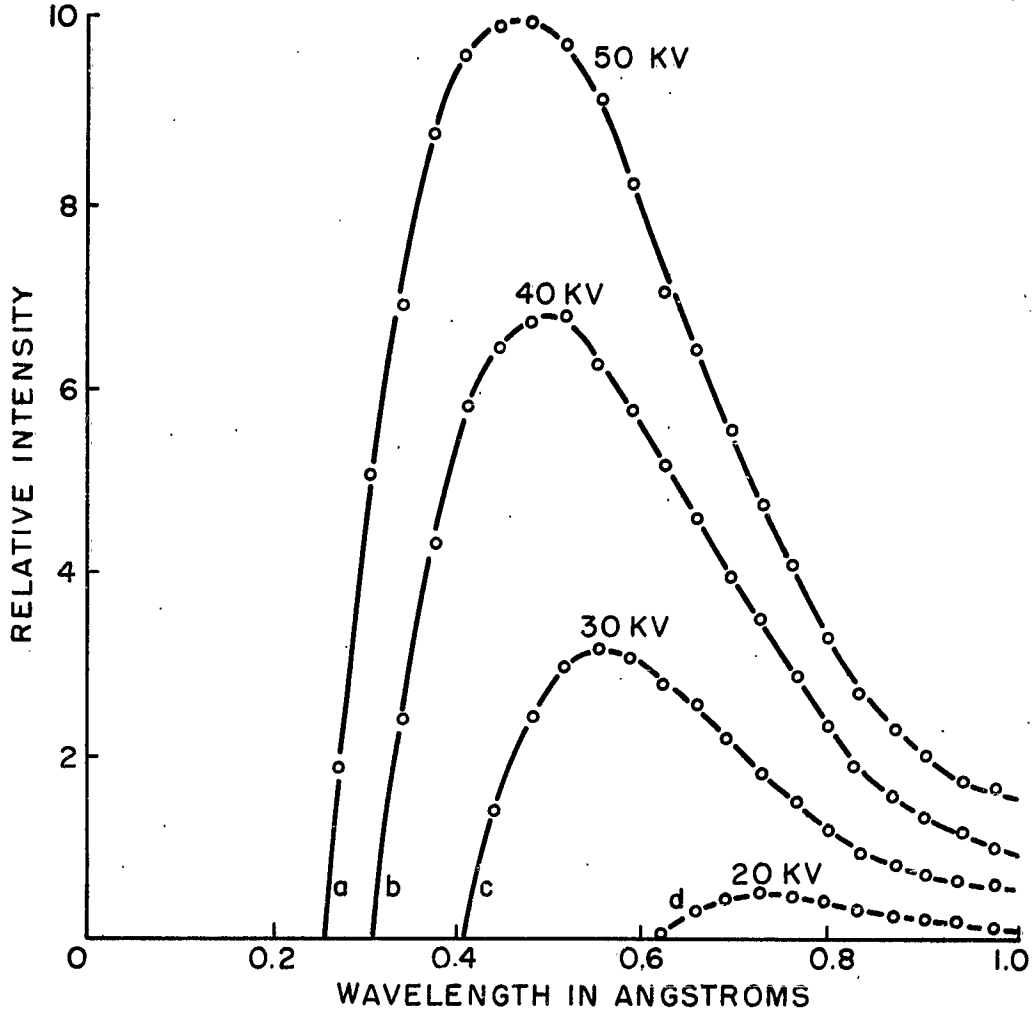

Figure 33. Relative Intensity versus Wavelength in Angstroms for a Tungsten Target at Various Voltages. (After measurements of Ulrey given by Richtmyer, Kennard, and Lauretsen.[9])

tinuous spectrum emitted by a thick target can be approximated by the continuous spectrum emitted by a thin target. The usual assumption is that the total emission from a thick target is obtained by considering a summation over each of the emissions from a series of thin targets one behind the other, with the energy of the incident electrons decreasing for each succeeding thin target.[10] In this discussion, however, we are not interested in the absolute value of the intensity of the continuous spectrum at a specific wavelength, but in the relative intensity transmitted through a given shield. Qualitative relations of the various parameters will therefore suffice.

The equations for the minimum wavelength and the intensity of radiation at a given wavelength in terms of the voltage and the current of the electron beam are:

$$\lambda_{min} = \frac{k}{V} \quad , \tag{5.16}$$

and[11]

$$J_\lambda = K \frac{1}{\lambda^2} \, i_1 \quad . \tag{5.17}$$

From Equations (5.16) and (5.17), one can write for two different wavelengths:

$$\frac{J_{\lambda 1}}{J_{\lambda 2}} = \left(\frac{V_1}{V_2}\right)^2 \left(\frac{i_1}{i_2}\right) \quad , \tag{5.18}$$

which can be transformed into

$$\frac{J_{\lambda 1}}{J_{\lambda 2}} = \left(\frac{v_1}{v_2}\right)^2 \frac{W_1}{W_2} \quad , \tag{5.19}$$

since

$$V = \frac{1}{2} \frac{m}{e} v^2 \quad , \tag{5.20}$$

where W_1 represents the kinetic energy corresponding to i_1 and v_1.

The transmission intensity varies exponentially with the mass absorption coefficient μ/ρ, the density, ρ, and the thickness, x, of the shield material, as,

$$\frac{J}{J_o} = e^{-\left(\frac{\mu}{\rho}\right)_{\lambda_o} \rho x} \quad . \tag{5.21}$$

The mass absorption coefficient depends on the shield material and the wavelength λ, and is usually directly proportional to the density and inversely proportional to the wavelength. Mass absorption coefficients are determined experimentally and are given in the literature.

If a reference intensity at a given wavelength is chosen, then from Equations (5.19) and (5.21), one has

$$\frac{J}{J_{ref}} = e^{-\left(\frac{\mu}{\rho}\right)_{\lambda_n} \rho x} \cdot \left(\frac{v_n}{v_{ref}}\right)^2 \frac{W_n}{W_{ref}} \quad . \tag{5.22}$$

Since the present work is intended to apply to high-power klystrons, a d-c beam voltage of 250 kv is chosen for the two-cavity klystron for the following computations. It is seen from Figures (24e) and (25e) that the maximum percentage of Δq and the maximum percentage of ΔW are those of velocity-class 1.2. The intensity of radiation from this velocity-class of electrons, therefore, is taken as the reference intensity. The

material of the shield is lead ($\rho = 11.005$ gr/cm^3) and the thickness of it is assumed to be such as to drop the reference intensity to $1/e$ of its incident magnitude. The mass absorption coefficients for lead are plotted in Figure (34), in the wavelength range of interest.[12] Equation (5.21), then, gives

$$\frac{J}{J_{ref}} = e^{-.4 \times 11.005\, x} = \frac{1}{e}$$

$$x = .22717 \text{ cm.}$$

This thickness of .22717 cm and Equation (5.22) are used in the rest of the computations. The results are tabulated in Table III.

It is seen from Table III that the maximum transmitted intensity with the velocity-filter gap is less than the maximum transmitted intensity (the reference) without it.

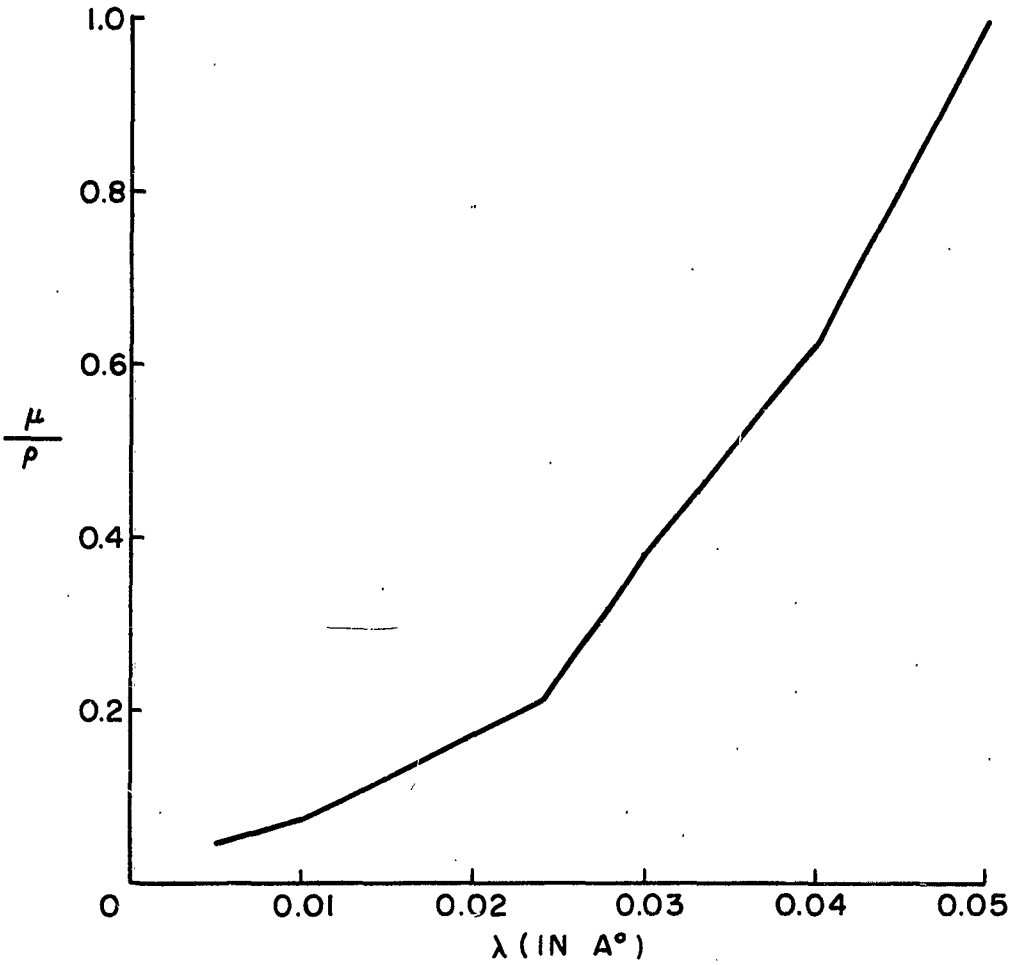

Figure 34. Mass Absorption Coefficient μ/ρ versus Wavelength in Angstroms for Lead Shield.

TABLE III.

Ratios of the Transmitted Intensity to the Reference Intensity with and without the Velocity-Filter Gap.

	Velocity-class	Equivalent voltage in kv	Minimum Wavelength λ_{min} in A°	Mass absorption coefficient (μ/ρ)	Kinetic energy	Transmitted intensity J/J_{ref}
Without velocity-filter gap	1.0 – 1.1	275.6	.0435	.7520	.315004	.022377
	1.1 – 1.2	330.6	.0363	.5300	1.021034	.151560
	1.2 – 1.3	390.6	.0307	.4000	1.515621	.367879*
	1.3 – 1.4	455.6	.0263	.2555	.168071	.068294
With velocity-filter gap	1.0 – 1.1	275.6	.0435	.7520	.872499	.061981
	1.1 – 1.2	330.6	.0363	.5300	1.257900	.186720
	1.3 – 1.4	455.6	.0263	.2555	.217011	.088181
	1.4 – 1.5	525.6	.0228	.1810	.448031	.252997†

*Reference

† Accelerated Class 3 electrons

VI. CONCLUSIONS AND RECOMMENDATIONS

A. CONCLUSIONS

Although this study was based on a very simple model, many interesting and important results were obtained, which may serve as guides for future investigations. Conclusions from this ballistic analysis can be grouped under: (1) exact graphic analysis and its approximation, which includes the first gap and the first drift space, and (2) computer solutions, which includes the second gap, the second drift space, and the third gap.

1. Exact Graphic Analysis and Its Approximation

Exact graphic analysis reveals the physical relationships in the first gap and in the drift space, but it is tedious and time consuming and does not give the functional relationships between the various parameters. Approximating the graphic method analytically, on the other hand, is demonstrated to be valid, the second-order method both approximating the large-signal cases well and also giving analytical formulas that reveal information about the harmonics.

In the first gap both velocity and current modulations are produced during the passage of the electron beam through the gap, and the transit time plays an important role in these phenomena. The velocity modulation is proportional to the depth of modulation α_1, but is inversely proportional to the d-c gap transit angle θ_{g_1}. The difference between the minimum velocity and d-c velocity is greater than the corresponding difference between the maximum velocity and the d-c velocity. Like the velocity modulation, the current modulation is also proportional to the depth of modulation,

but it varies with the d-c gap transit angle, first increasing and then decreasing. Both velocity and current expressions contain harmonics at the exit from the first gap, but this effect is more pronounced in the expression for the current.

In the first drift space, density modulation is produced in a velocity-modulated electron beam through drift action. The beam current develops harmonics, and the amplitudes of harmonics are proportional to the depth of modulation. The maximum value of the fundamental current is seen to be greater than the value of 1.16 predicted by Webber.[5] The point in the drift space at which the maximum value of a harmonic occurs is inversely proportional to the depth of modulation. As the depth of modulation is increased, two bunches of electrons occur, one of fast electrons (Class 1) and the other of slow electrons (Class 2). These results have been shown, at least qualitatively, in the works of others. An additional phase angle β_n is introduced into the current by the two independent components of each harmonic. The velocity becomes more nonlinear at the end of the drift space (overtaking occurs), but its extreme values do not change.

2. Computer Solutions

The multivalued nature of transit times and the occurrence of overtaking make it impossible to derive explicit analytical formulas for the velocity and the current of the electron beam at the second gap and beyond; thus one is limited to graphic analysis, i.e., the digital computer solutions. One salient point in the formulation of the computer problems is consideration of the components instead of the total contributions of current from the increments of ωt_c time. This causes all the time derivatives to be single-valued.

The graphic analysis revealed that one cannot easily predict the operating parameters for a catcher-gap without calculating the kinetic energies at the entrance of the gap and at the exit from it. It was seen that the electron beam debunches as the operating parameters are adjusted for maximum energy extraction. This is also shown by Webber.[13] Optimum operating parameters for the catcher-gap of a two-cavity klystron were found to be $\theta_{g_2} = \pi/2$ radians, $\Gamma_2 = -\pi/4$ radian. The maximum efficiency was 23.995 per cent for $\alpha_1 = 0.8$ and $\alpha_2 = 1.0$ with the selected initial conditions of $\theta_{g_1} = 1.75$ radians and $\theta_{o1} = 2\pi$ radians.

The operating parameters for a velocity-filter gap used as the second gap were easily predicted by the decrease in the maximum velocity at the exit from the gap. The optimum values were found to be $\theta_{g_2} = 7\pi/4$ radians and $\Gamma_2 = -\pi/2$ radians. This gap, which is a rather long gap, showed interaction with the fast electrons (Class 1). The electron beam became more bunched in passing through the gap.

Even with the velocity-filter gap as a third gap in combination with the two-cavity klystron, Class 3 electrons showed undesirable behavior. This was a result of their being at the same velocity as Class 1 electrons and almost half a cycle apart from them. The drifting of the electron beam in the second drift space, therefore, did not alter their relative positions with respect to each other. Consequently, in the third gap, with the known operating parameters for the velocity-filter gap, Class 3 electrons were accelerated while Class 1 electrons were decelerated. This resulted in a greater maximum velocity at the exit from the third gap than that at the exit from the catcher-gap. It was shown, however, that the inclusion of the velocity-filter gap was an improvement so far as the intensities of the X-ray

radiation transmitted through a given shield were concerned (see Table II), since the amount of charge of Class 1 electrons was very much larger than that of Class 3 electrons. To obtain the greatest decrease in the velocity of Class 1 electrons, the optimum second drift length was found to be $\theta_{o2} = 9\pi/4$ radians. Under these operating conditions, an efficiency of 5.368 per cent was obtained for $\alpha_3 = 1.0$. Thus it was demonstrated that the idea of interaction of a r-f gap with a group of bunched electrons having a specific velocity-class is feasible.

B. RECOMMENDATIONS

The combination of the two-cavity klystron and the velocity-filter gap partly solves the problem of X-ray radiation resulting from the acceleration of Class 3 electrons. Since their velocities are greater than those of Class 1 electrons at the exit from the third gap, the relative positions of these classes will alter in a third drift space. In fact, an additional optimum drift space can be introduced such that Class 1 electrons and Class 3 electrons come to the same phase. Inclusion of an additional velocity-filter gap at the end of this optimum drift space obviously will further decrease the velocity of this new group of electrons and hence the X-ray radiation. A number of alternating drift spaces and velocity-filter gaps may completely reduce the radiation to safe levels.

The acceleration of Class 3 electrons can be avoided by tuning the velocity-filter gap to the second harmonic of the beam current. The phase of the induced voltage across the gap can be adjusted such that the r-f field interacts with both Class 1 electrons and Class 3 electrons in the decelerating half cycle.

Experimental verification of the results obtained in the analysis of this report can be made on a device such as the dynamic beam tester.[7] Although there will be discrepancies between experimental and analytical results because of the limitations of the model, qualitative agreement between the two is expected.

The model used in the above analysis was a simple one. The same kind of analysis can be applied to a model that has gridless gaps, finite size, and that is modified for space charge.

APPENDIX A.

INITIAL CONDITIONS AT ENTRANCE TO SECOND GAP (PLANE C)

(θ_{g_1} = 1.75 radians, a_1 = 0.8, θ_{o_1} = 2π radians)

Electron no. n	Time ωt_c	Normalized velocity v_c/v_o	Normalized component current i_c/I_o	Electron no. n	Time ωt_c	Normalized velocity v_c/v_o	Normalized component current i_c/I_o	Electron no. n	Time ωt_c	Normalized velocity v_c/v_o	Normalized component current i_c/I_o
1	.200	.720648	.203387	24	.200	.949176	.905942	47	1.800	1.158969	.313954
2	.400	.708945	.212843	25	6.283185	1.002564	1.095834	48	1.850	1.152639	.308198
3	.600	.697773	.225171	26	6.200	1.028247	1.219381	49	1.900	1.146321	.302669
4	.800	.687152	.241524	27	6.100	1.063077	1.439242	50	1.950	1.140026	.297364
5	1.000	.677133	.263860	28	6.000	1.104585	1.833450	51	2.000	1.133753	.292266
6	1.200	.667783	.295909	29	5.950	1.129547	2.197772	52	2.050	1.127498	.287364
7	1.400	.659251	.345734	30	5.900	1.159782	2.907187	53	2.100	1.121268	.282651
8	1.600	.651865	.435440	31	5.850	1.203425	5.629951	54	2.600	1.060626	.244266
9	1.800	.646592	.664387	32	5.850	1.283080	5.602494	55	3.100	1.003609	.217866
10	1.850	.645978	.802519	33	5.900	1.310843	2.871670	56	3.600	.950649	.199819
11	1.900	.646026	1.073562	34	5.950	1.325186	2.157251	57	4.100	.901822	.188030
12	1.950	.647827	2.093169	35	6.000	1.334324	1.786587	58	5.100	.815991	.179293
13	1.950	.660110	2.336703	36	6.100	1.344292	1.381072	59	5.700	.771490	.183311
14	1.900	.669454	1.323102	37	6.200	1.347779	1.150158	60	5.800	.764551	.184778
15	1.850	.677165	1.056814	38	6.283185	1.347535	1.017763	61	5.850	.761131	.185612
16	1.800	.684316	.923765	39	.200	1.339406	.806984	62	5.900	.757744	.186515
17	1.600	.711270	.718130	40	.400	1.324428	.672960	63	5.950	.754390	.187489
18	1.400	.738150	.655712	41	.600	1.305240	.578237	64	6.000	.751069	.188539
19	1.200	.766213	.638434	42	.800	1.283352	.507024	65	6.100	.744524	.190877
20	1.000	.796131	.645942	43	1.000	1.259747	.451353	66	6.200	.738109	.193561
21	.800	.828537	.672874	44	1.200	1.235092	.406631	67	6.283185	.732873	.196082
22	.600	.864128	.719896	45	1.400	1.209862	.369996				
23	.400	.903861	.792801	46	1.600	1.184403	.339546				

REFERENCES

1. D. L. Webster, "Cathode Ray Bunching," Jour. Appl. Phys., 10 (July 1939), pp. 501-508.

2. T. G. Mihran, "The Effect of Space Charge on Bunching in a Two-Cavity Klystron," I. R. E. Trans., ED-6 (January 1959).

3. G. C. Dalman, Unpublished work.

4. H. B. Dwight, Tables of Integrals and Other Mathematical Data, New York: Macmillan (1953), pp. 174-191.

5. S. E. Webber, "Ballistic Analysis of a Two-Cavity Finite Beam Klystron," I. R. E. Trans., ED-5 (April 1958), pp. 98-108.

6. L. Solymar, "Exact Solutions of the One-Dimensional Bunching Problem," Jour. Elect. Control, 10 (March 1961).

7. A. S. Gilmour, Jr., "A Beam Tester for Studying the Characteristics of D-C and Velocity-modulated Electron Beams," Research Report EE 495, Cornell University (May 1961).

8. A. H. Compton, X-Rays and Electrons, New York: D. Van Nostrand (1928), pp. 27-28.

9. F. K. Richtmyer, E. H. Kennard, and T. Lauritsen, Introduction to Modern Physics, New York: McGraw-Hill (1955), pp. 374-377.

10. S. Flugge, Handbuch der Physik, Vol. 30, Berlin: Springer (1957), p. 349.

11. "High-Power Tube Program," Semiannual Technical Summary Report to ARPA(U), Lincoln Laboratory, M.I.T. (30 June 1962), p. 19.

12. C. D. Hodgman, Handbook of Chemistry and Physics, Cleveland; Clemical Rubber (1952), p. 2240.

13. S. E. Webber, "Some Calculations on the Large Signal Energy Exchange Mechanisms in Linear Beam Tubes," I.R.E. Trans., ED-7 (July 1960), pp. 154-162.